Cosmic-ray acceleration and escape from supernova remnants

Monthly Notices
of the
ROYAL ASTRONOMICAL SOCIETY

MNRAS **431,** 415–429 (2013)
Advance Access publication 2013 February 27

doi:10.1093/mnras/stt179

Cosmic-ray acceleration and escape from supernova remnants

A. R. Bell,⋆ K. M. Schure, B. Reville and G. Giacinti

Clarendon Laboratory, University of Oxford, Parks Road, Oxford OX1 3PU, UK

Accepted 2013 January 28. Received 2013 January 23; in original form 2012 November 22

ABSTRACT

Galactic cosmic-ray (CR) acceleration to the knee in the spectrum at a few PeV is only possible if the magnetic field ahead of a supernova remnant (SNR) shock is strongly amplified by CRs escaping the SNR. A model formulated in terms of the electric charge carried by escaping CRs predicts the maximum CR energy and the energy spectrum of CRs released into the surrounding medium. We find that historical SNRs such as Cas A, Tycho and Kepler may be expanding too slowly to accelerate CRs to the knee at the present time.

Key words: acceleration of particles – magnetic fields – shock waves – cosmic rays – ISM: supernova remnants.

1 INTRODUCTION

During diffusive shock acceleration (DSA) cosmic rays (CRs) gain energy by repeatedly passing back and forth between the upstream and downstream plasmas (Axford, Leer & Skadron 1977; Krymskii 1977; Bell 1978; Blandford & Ostriker 1978). CRs diffuse ahead of the shock to form a precursor with an exponential scaleheight $D_\mathrm{u}/u_\mathrm{s}$, where u_s is the shock velocity and D_u is the CR diffusion coefficient upstream of the shock. The average dwell-time spent upstream of the shock between successive shock crossings is $4D_\mathrm{u}/cu_\mathrm{s}$ for relativistic particles (Bell 2012). This, along with the corresponding downstream dwell-time, determines the rate at which CRs are accelerated. Lagage & Cesarsky (1983a,b) showed that the time taken for CR acceleration is $t_\mathrm{accel} = 4D_\mathrm{u}/u_\mathrm{s}^2 + 4D_\mathrm{d}/u_\mathrm{d}^2$, where D_d is the downstream diffusion coefficient and u_d is the downstream fluid velocity in the shock rest frame. Since $u_\mathrm{d} = u_\mathrm{s}/4$ for a strong shock, it might appear that the downstream dwell-time determines the acceleration rate, but we can expect $D_\mathrm{d} \ll D_\mathrm{u}$ partly because the magnetic field is increased by compression by the shock, partly because the compressed downstream magnetic field is more closely perpendicular to the shock normal, and partly because the downstream field is disturbed and more irregular after passing through the shock. If the downstream and upstream dwell-times are the same, $t_\mathrm{accel} = 8D_\mathrm{u}/u_\mathrm{s}^2$. A further common assumption is that Bohm diffusion applies: $D_\mathrm{u} = cr_\mathrm{g}$ or $D_\mathrm{u} = cr_\mathrm{g}/3$, where r_g is the CR Larmor radius. This assumes a diffusion model in which CRs are scattered by irregularities in the magnetic field such that the scattering mean free path is of the order of the CR Larmor radius. There is some observational evidence for Bohm diffusion (Stage et al. 2006; Uchiyama et al. 2007). Furthermore, if the mean free path were much larger than a Larmor radius, acceleration by a supernova remnant (SNR) to the knee in the Galactic CR spectrum would be very difficult. The maximum CR energy is determined by the condition that t_accel cannot exceed the age t_SNR of a SNR (Lagage & Cesarsky 1983a,b). Assuming $D_\mathrm{u} = cr_\mathrm{g}$, the maximum CR energy T_max in eV is given by $T_\mathrm{max} = 0.03 B_{\mu\mathrm{G}} u_7^2 t_{1000}$ PeV, where $B_{\mu\mathrm{G}}$ is the upstream magnetic field in microgauss, u_7 is the shock velocity in units of $10\,000\,\mathrm{km\,s^{-1}}$ and t_{1000} is the SNR age in thousands of years. For a typical young SNR expanding into the interstellar medium (ISM) without magnetic field amplification, $B_{\mu\mathrm{G}} = 3$, $u_7 = 0.5$ and $t_{1000} = 0.4$, giving $T_\mathrm{max} = 0.01$ PeV which falls a factor of $\sim$100 short of that required to explain the Galactic CR spectrum. SNRs in the Sedov phase do not fare better. Their shock velocities decrease in proportion to time$^{-3/5}$ and radius$^{-3/2}$, so little benefit accrues from their larger age and radius. This posed a serious problem for DSA as an explanation of the Galactic spectrum until it was shown that a plasma instability driven by streaming CRs in the upstream precursor could amplify the magnetic field ahead of the shock and facilitate rapid acceleration to higher energies (Lucek & Bell 2000; Bell 2004, 2005).

The phenomenon of magnetic field amplification provides a mechanism by which the CR energy can be raised significantly beyond 0.01 PeV, but there remains the question of why the fields are amplified to the observed magnitude, up to hundreds of μG in the historical SNR (Berezhko, Ksenofontov & Völk 2003; Vink & Laming 2003; Völk, Berezhko & Ksenofontov 2005), and why CRs are accelerated to a few PeV rather than 0.1 or 10 PeV. We try to answer these questions by examining the self-consistent interaction between streaming CRs, behaving kinetically, and the upstream plasma behaving magnetohydrodynamically.

It has been known for many years that the escape of CRs upstream of the shock is an important part of the overall acceleration process as discussed below in the final paragraphs of Section 3. We find that the combined CR–magnetohydrodynamics (CR–MHD) system organizes itself to allow a suitable number of CRs to escape upstream. The CRs drive magnetic field amplification which in turn regulates the number of escaping CRs. If a smaller number of CRs escaped, the magnetic field would be insufficiently amplified to confine and accelerate the CRs. If a larger number of CRs escaped, the

⋆ E-mail: t.bell1@physics.ox.ac.uk

magnetic field would grow too rapidly to allow their escape. Hence, a self-regulating system is set up that determines the number and maximum energy of escaping CRs.

The paper is organized as follows. Sections 2 and 3 present approximate calculations showing how a limit on the CR energy is placed by the need for CRs to drive magnetic field amplification by escaping upstream. Sections 4–7 describe Vlasov–Fokker–Planck (VFP) simulations that support the arguments of Sections 2 and 3. Sections 8–11 apply the results to SNRs and the Galactic CR spectrum. Readers unfamiliar with VFP simulations may wish to read Sections 1–3 and 8–11 before returning to the computational validation and illustration in Sections 4–7.

2 CONDITIONS FOR STRONG MAGNETIC FIELD AMPLIFICATION

We assume that magnetic field is generated by the non-resonant hybrid (NRH) instability described by Bell (2004). This is one of a class of plasma instabilities driven by CR streaming. In its simplest form, CRs have a Larmor radius much greater than the wavelength of spiral perturbations in a zeroth-order uniform magnetic field. Because of their large Larmor radius, the streaming CRs, carrying an electric current density $\boldsymbol{j}_{\rm CR}$, are essentially undeflected by the perturbed field but the $\boldsymbol{j}_{\rm CR}\times\boldsymbol{B}$ force acts towards the centre of the spiral. A corresponding reactive force acts on the background plasma to expand the spiral. This stretches and increases the magnitude of the perturbed magnetic field, thereby increasing the $\boldsymbol{j}_{\rm CR}\times\boldsymbol{B}$ force in a positive feedback loop that drives the instability. NRH appears to be the most rapidly growing instability driven by CRs streaming on a relevant scalelength. Other instabilities that have attracted significant attention are the resonant Alfvén instability (Kulsrud & Pearce 1969; Wentzel 1974) that grows with spatial wavelengths spatially resonant with the CR Larmor radius and the Weibel instability (Weibel 1959) that grows quickly on the spatial scale of an electron or proton collisionless skin depth, $c/\omega_{\rm pe}=5.3(n_{\rm e}/{\rm cm}^{-3})^{-1/2}\,{\rm km}$, $c/\omega_{\rm pi}=\sqrt{m_{\rm p}/m_{\rm e}}c/\omega_{\rm pe}$. The Weibel instability is important for interactions engaging thermal or mildly suprathermal electrons and ions, and may be effective for CR acceleration to low energies, but it grows on a scale too small to scatter PeV ions which have a Larmor radius of $\sim10^9c/\omega_{\rm pe}$. The Alfvén instability grows on the desired spatial scale but grows less quickly than the NRH instability in the SNR shock environment. Instabilities that grow on scales larger than the CR Larmor radius (Drury & Falle 1986; Malkov & Diamond 2009; Bykov, Osipov & Ellison 2011; Schure & Bell 2011; Drury & Downes 2012; Rogachevskii et al. 2012) tend to have longer growth times but turbulent amplification may increase the growth rate (Bykov et al. 2011). An extended discussion of instabilities driven by CRs streaming can be found in Schure et al. (2012).

From the Lagage & Cesarsky (1983a,b) limit as described in Section 1, it is clear that proton acceleration to a few PeV is only possible if the magnetic field is strongly amplified above its characteristic interstellar value of a few μG. The following argument places an upper limit on the maximum energy of a CR that can be strongly scattered by a magnetic field growing on the scale of a CR Larmor radius. The background thermal plasma is highly magnetized on the scale of a PeV CR Larmor radius. Consequently, the magnetic field is 'frozen in' to the thermal plasma. Magnetic field amplification occurs as the plasma moves and stretches field lines. Assuming the perturbed magnetic field does not far exceed the initial field, the $\boldsymbol{j}_{\rm CR}\times\boldsymbol{B}$ force displaces a plasma element a maximum distance $s_{\rm max}\sim(j_{\rm CR}Bt^2)/2\rho$ in time t where $\boldsymbol{B}$ is the initial seed field. For the stretched magnetic field to strongly scatter CRs as required for Bohm diffusion, the displacement must grow to the order of a CR Larmor radius, that is, $s_{\rm max}\sim T/cB$, where T is the CR energy in eV. The CR current density $\boldsymbol{j}_{\rm CR}$ carries an energy flux $\boldsymbol{j}_{\rm CR}T$ in the upstream plasma rest frame which cannot far exceed the energy flux $\rho u_{\rm s}^3/2$ carried by the upstream plasma into the shock, where ρ is the upstream mass density. We define a CR acceleration efficiency η such that $j_{\rm CR}T=\eta\rho u_{\rm s}^3$. We then have two equations: $s_{\rm max}=(j_{\rm CR}Bt^2)/2\rho\sim T/cB$ and $j_{\rm CR}=\eta\rho u_{\rm s}^3/T$. When combined, they yield a CR energy $T\sim(\eta cu_{\rm s}^3)^{1/2}Bt$. This expression for T is equivalent to $T\sim1.5(\eta u_7^3)^{1/2}B_{\mu\rm G}t_{1000}\,{\rm PeV}$, where u_7 is the shock velocity in units of $10\,000\,{\rm km\,s^{-1}}$, $B_{\mu\rm G}$ is the seed magnetic field in μG from which amplification begins, and t_{1000} is the time in thousands of years. Characteristically for young SNRs, $u_7=0.5$, $t_{1000}=0.4$, $\eta=0.03$ (see Appendix A) and $B_{\mu\rm G}=3$ where the magnetic field of a few μG represents the seed field from which the instability grows. With these estimates, $T\sim0.1\,{\rm PeV}$, which is an order of magnitude less than the energy of the knee. This estimate is independent of any detailed instability theory except for the assumption that magnetic field amplification takes place through plasma motions generated by the $\boldsymbol{j}_{\rm CR}\times\boldsymbol{B}$ force acting on the scale of a CR Larmor radius. It highlights the difficulty of amplifying magnetic field by orders of magnitude on the scale of the Larmor radius of a PeV proton and the need for an instability that can provide non-linear growth of the magnetic field.

The NRH instability offers a way round this difficulty by initially growing very rapidly on a scale much less than the CR Larmor radius. Since the small-scale magnetic field grows unstably, the $\boldsymbol{j}_{\rm CR}\times\boldsymbol{B}$ force grows exponentially in time. The scale-size increases to the CR Larmor radius during non-linear growth. The NRH growth rate is $\gamma=(kj_{\rm CR}B_0/\rho)^{1/2}$, where B_0 is the zeroth-order magnetic field and k is the wavenumber on which the instability grows. The maximum NRH growth rate is $\gamma_{\rm max}=0.5j_{\rm CR}(\mu_0/\rho)^{1/2}$ which occurs at a wavenumber $k_{\rm max}=0.5\mu_0j_{\rm CR}/B_0$. $\gamma_{\rm max}$ is $(k_{\rm max}r_{\rm g})^{1/2}$ times larger than the NRH growth rate for $kr_{\rm g}=1$, thus allowing the magnetic field and the $\boldsymbol{j}_{\rm CR}\times\boldsymbol{B}$ force to increase rapidly. The NRH and Alfvén growth rates are similar at $kr_{\rm g}=1$ (see Appendix E and Bell 2004). Using the above nomenclature, $k_{\rm max}r_{\rm g}=\eta u_{\rm s}^3/cv_{\rm A}^2=2\times10^4\eta_{0.03}u_7^3n_{\rm e}B_{\mu\rm G}^{-2}$, where $v_{\rm A}$ is the Alfvén speed, $\eta=0.03\eta_{0.03}$ and $n_{\rm e}$ is the electron density in ${\rm cm}^{-3}$. For a discussion of the value of η, see Appendix A and Bell (2004). The growth time of the fastest growing mode is then $\gamma_{\rm max}^{-1}=50\eta_{0.03^{-1}}n_{\rm e}^{-1/2}u_7^{-3}T_{\rm PeV}\,{\rm yr}$, where $T_{\rm PeV}$ is the energy in PeV of the CR driving the instability. $\gamma_{\rm max}^{-1}=400\,{\rm yr}$ for $\eta_{0.03}=1$, $n_{\rm e}=1$, $u_7=0.5$ which implies that even the NRH instability struggles to amplify the magnetic field sufficiently to accelerate CRs to PeV energies in the historical SNR. For growth by many e-foldings, the NRH instability must be driven by CRs with energies less than 1 PeV.

As remarked above, the fastest growing mode grows on a scale $k_{\rm max}^{-1}$, whereas efficient CR scattering requires fluctuations in the magnetic field on a scale $r_{\rm g}$. The above analysis showed that $k_{\rm max}r_{\rm g}=2\times10^4\eta_{0.03}u_7^3n_{\rm e}B_{\mu\rm G}^{-2}$. The instability initially grows on a scale too small to effectively scatter PeV CRs. Two factors save the situation. First, as the magnetic field grows from a few μG to a few hundred μG, the CR Larmor radius decreases by the corresponding factor of ∼100. Secondly, the characteristic scalelength of the structured magnetic field increases during non-linear growth of the instability. Fig. 1 is drawn from figs 3 and 4 of Bell (2004). The graph of energy densities shows how the magnitude of the magnetic field grows to many times its seed value in a time $\sim10\gamma_{\rm max}^{-1}$. The characteristic scalelength grows during this time as shown by the grey-scale images. By the time $t=10$ the scalelength has grown to the size of the computational box from its initially much smaller

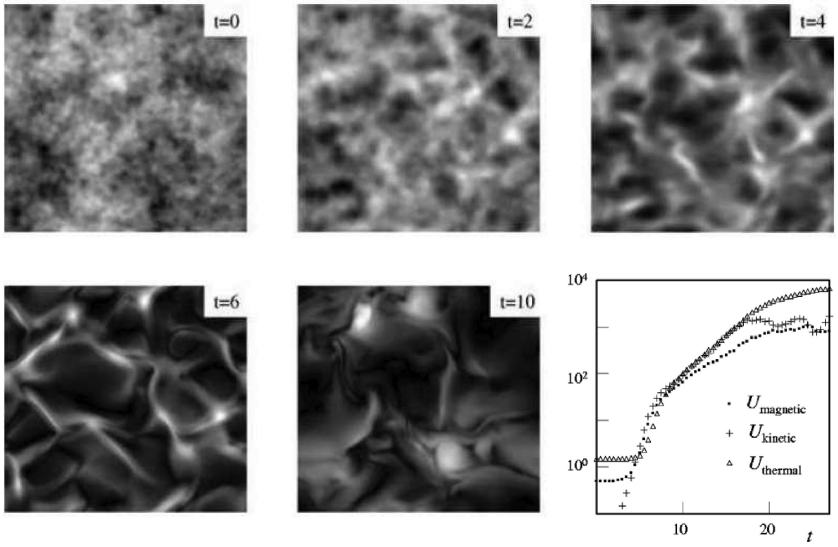

Figure 1. Plots of the magnitude of a magnetic field driven by CRs streaming into the page (2D slices of a 3D simulation). The field grows from noise on a small spatial scale at $t = 0$. By $t = 10$ the spatial scale has grown to the size of the computational box. The graph shows how the mean magnetic, kinetic and thermal energy densities increase with time. This figure is composed from figs 3 and 4 of Bell (2004) where further details can be found. The units of time are such that $\gamma_{\rm max} = 1.26$.

scale. Both k and $r_{\rm g}$ decrease by a large factor by the time $10\gamma_{\rm max}^{-1}$. The simulation reproduced in Fig. 1 had a fixed CR current so it was impossible to demonstrate strong CR scattering by the magnetic field after $t = 10\gamma_{\rm max}^{-1}$, but the figure provides strong evidence for rapid initial growth of the fastest growing modes into large-scale magnetic structures able to scatter CRs on the scale of a Larmor radius.

3 COSMIC-RAY ESCAPE UPSTREAM OF THE SHOCK

The previous section does not provide an estimate of the magnitude of the amplified magnetic field, but it does define conditions under which strong magnetic field amplification occurs. CR acceleration to PeV energies requires strong magnetic field amplification which fixes the number of instability e-foldings in the range 5–10. This in turn fixes the CR current. From Fig. 1 we take the condition for strong magnetic field amplification in a particular volume of upstream plasma to be that $\int \gamma_{\rm max} {\rm d}t \sim 5$ in the time before the shock overtakes it. Since $\gamma_{\rm max} = 0.5 j_{\rm CR}\sqrt{\mu_0/\rho}$, the condition for field amplification is

$$Q_{\rm CR} = \int j_{\rm CR} {\rm d}t = 10\sqrt{\rho/\mu_0}\,, \tag{1}$$

where $Q_{\rm CR}$ is the total electric charge of CRs passing through a unit surface area upstream of the shock before the shock arrives. (It makes no difference whether the CRs passing through the plasma have high or low energies. It is only the number of CRs escaping upstream that counts.) Since only the highest energy CRs escape, the areal charge $Q_{\rm CR}$ is carried by the highest energy CRs being accelerated. The Larmor radius of a PeV proton in the ISM is comparable with the radius of the historical SNR and its scattering mean free path is very much greater than the SNR radius. These escaping CRs pass into the ISM with a low probability of further encounters with the SNR shock. Strongly scattered CRs at lower energies are confined by the shock and are advected away downstream after acceleration.

Suppose that the CR distribution follows a p^{-4} power law up to a momentum $p_{\rm max}$, then in steady state the electrical current of CRs escaping in a small band of energies above the energy $eT_{\rm max} = cp_{\rm max}$ is

$$j_{\rm CR} = eu_{\rm s}\pi p_{\rm max}^3 f_0(p_{\rm max})\,, \tag{2}$$

where f_0 is the isotropic part of the CR distribution in momentum space at the shock. Equation (2) is derived from equation (11a) below by integrating in space across the shock and deriving the rate at which CRs reach the momentum $p_{\rm max}$. The derivation can be found in Appendix B. In comparison, the CR pressure at the shock, where the CR distribution extends down to $p = mc$ and m is the proton mass, is

$$P_{\rm CR} = \frac{4\pi}{3} c p_{\rm max}^4 f_0(p_{\rm max}) \ln\left(\frac{p_{\rm max}}{mc}\right)\,, \tag{3}$$

giving

$$j_{\rm CR} = 0.05\frac{u_{\rm s} P_{\rm CR}}{T_{\rm max}}\,, \tag{4}$$

where we have assumed $\ln(p_{\rm max}/mc) = 14$ for a CR distribution extending from 1 GeV to 1 PeV. The condition for magnetic field amplification that $\int j_{\rm CR}{\rm d}t = 10\sqrt{\rho/\mu_0}$ can be rearranged to give a value for $T_{\rm max}$:

$$T_{\rm max} = 0.005\frac{P_{\rm CR}}{\rho u_{\rm s}^2}\,\rho u_{\rm s}^3 t\sqrt{\frac{\mu_0}{\rho}}\,, \tag{5}$$

which is equivalent to

$$T_{\rm max} = 8\, n_{\rm e}^{1/2} u_7^3 t_{1000}\frac{P_{\rm CR}}{\rho u_{\rm s}^2}\,{\rm PeV}\,. \tag{6}$$

For characteristic values ($u_7 = 0.5, n_{\rm e} = 1, t = 0.4, P_{\rm CR}/\rho u_{\rm s}^2 = 0.3$) $T_{\rm max} \sim 100$ TeV. As expected from the above discussion, this falls short of the few PeV required to explain Galactic CRs. This will be discussed further in Section 8.

Zirakashvili & Ptuskin (2008) and Zirakashvili, Ptuskin & Völk (2008) developed a related analytic model of the excitation of the NRH instability and CR confinement upstream of the shock. They

derived an estimate for the maximum CR energy with a similar dependency on $n_e^{1/2}u^3t$ in the numerator of their equation (19) but with an additional denominator that depends on the magnitude of the amplified magnetic field. Their analysis operates at a more detailed level than ours since they consider the growth in amplitude of the amplified magnetic field over a range of scales and small angle CR scattering by small-scale field. However, the dominant physics is similar in their analysis and ours, and their estimate of the CR energy (equation 19) is similar to that in our equation (6).

Note that the magnetic field does not enter into the estimation of the maximum energy CR in equation (6). The magnetic field is assumed to grow to whatever magnitude and spatial scale required to confine CRs at energies less than $T_{\max}$. This assumption is justified on the basis that the magnitude of the field increases by a substantial numerical factor in time $\gamma_{\max}^{-1}$ even in the non-linear regime and that this is accompanied by rapid growth in characteristic spatial scale. For example, the magnetic field and its spatial scale are very much larger in Fig. 1 when $\int \gamma_{\max} \mathrm{d}t \approx 8$ than when $\int \gamma_{\max} \mathrm{d}t \approx 5$ even though the time is different by a factor of only 1.6. Allowing the field to grow for just a little longer gives a much larger magnetic field and spatial scale. Consequently, the primary parameter is not the magnitude of the magnetic field but the charge carried by escaping CRs.

It is clear that magnetic field amplification is only possible if a population of high-energy CRs escape upstream of the shock. A magnetic field capable of stopping their escape is only produced after the areal charge Q_{CR} has escaped. Thus, CR escape upstream of the shock is an essential aspect of DSA when magnetic field amplification is operational. If a charge Q_{CR} has not passed through a particular point upstream of the shock, then CRs cannot be confined at that distance from the shock.

Previous authors have also concluded that CR escape upstream is inevitable, but generally for different reasons. One possibility is that CRs escape through filamentary cavities in the magnetic field (Reville & Bell 2012, 2013) but usually it is assumed that CRs escape at a free-escape boundary in position or momentum. Free-escape boundaries were introduced at an early stage in the development of shock acceleration theory (Ellison, Jones & Eichler 1981). It was appreciated that steady-state models were impossible without CR escape (Ellison & Eichler 1984; Berezhko & Ellison 1999; Malkov, Diamond & Völk 2000). The standard T^{-2} test particle energy spectrum at strong shocks diverges if integrated to infinite energy. The divergence is even stronger if non-linear CR feedback on to the shock structure is included since the relativistic CR pressure increases the density jump at the shock resulting in a spectrum flatter than T^{-2} at high CR energy. However, the conditions for a steady-state solution do not present a compelling argument for a free-escape boundary since time-dependent solutions offer an acceptable option. Indeed the Lagage & Cesarsky limit on CR energy is based on the assumption that the maximum CR energy increases with time. The case for CR escape was strengthened by the recognition that magnetic field amplification is essential since there will always be a distance upstream at which amplification is inoperative and CRs must escape. Similarly, there must always be an upper limit to the spatial scale to which field is amplified and a corresponding limit, through the Larmor radius, on the momentum to which CRs can be accelerated. This led to the imposition of a free-escape boundary either at an imposed distance upstream of the shock (e.g. Caprioli, Blasi & Amato 2010b; Ohira, Mirase & Yamazaki 2010) or at an imposed CR momentum (e.g. Ellison & Bykov 2011). Whether the free-escape boundary is imposed in momentum or configuration space, the momentum at which CRs escape depends on the magnetic field. Some authors (e.g. Ptuskin, Zirakashvili & Seo 2010) assume that the field is amplified until the magnetic energy density reaches a given fraction of ρu_s^2. The fractional magnetic energy density can be chosen to match observation (Völk et al. 2005; Ptuskin et al. 2010). Alternatively the field can be chosen to match the saturation value estimated by Bell (2004). Others (Caprioli, Blasi & Amato 2010a; Drury 2011) choose a mathematical form for the amplified magnetic field that allows for multiple possibilities. Ptuskin & Zirakashvili (2003), Caprioli, Blasi & Amato (2009a) and Caprioli et al. (2009b, 2010b) include magnetic field generation due to the resonant instability as it develops ahead of the shock. Vladimirov, Ellison & Bykov (2006) include magnetic field generation in response to gradients in the CR pressure. Ellison et al. (2012) choose an amplified magnetic field suitable for SNR expansion into a circumstellar wind.

In contrast to the above, CR escape in our model is determined by the escaping CR electric charge rather than the magnetic field generated in the upstream plasma, although magnetic field amplification is implicitly required by our model. Reville, Kirk & Duffy (2009) also used the escaping flux to calculate growth rates in an effort to motivate a realistic free-escape boundary location in their steady-state non-linear model. Their discussion on self-regulation of CR precursors, however, did not extend to the maximum CR energy.

4 A NUMERICAL MODEL

We now set out to test the above conclusions as far as we are able with a numerical model that includes the self-consistent interaction of CRs modelled kinetically with a background plasma modelled magnetohydrodynamically. Standard MHD equations describe the background plasma except that a $-\boldsymbol{j}_{\mathrm{CR}} \times \boldsymbol{B}$ force is added to the momentum equation:

$$\rho \frac{\mathrm{d}\boldsymbol{u}}{\mathrm{d}t} = -\nabla P - \frac{1}{\mu_0}\boldsymbol{B} \times (\nabla \times \boldsymbol{B}) - \boldsymbol{j}_{\mathrm{CR}} \times \boldsymbol{B} \tag{7}$$

as described in Lucek & Bell (2000) and Bell (2004). The CR distribution function $f(\boldsymbol{r}, \boldsymbol{p}, t)$ at position $\boldsymbol{r}$ and momentum $\boldsymbol{p}$ is defined in the local fluid rest frame and evolves according to the VFP equation

$$\frac{\mathrm{d}f}{\mathrm{d}t} = -v_i \frac{\partial f}{\partial r_i} + p_i \frac{\partial u_j}{\partial r_i}\frac{\partial f}{\partial p_j} - \epsilon_{ijk} e v_i B_j \frac{\partial f}{\partial p_k} + C(f), \tag{8}$$

where $C(f)$ is an optional collision term included to represent scattering by magnetic fluctuations on a small scale. The electric field is zero in the local fluid rest frame. Quadratic terms in the local fluid velocity $\boldsymbol{u}$ are neglected on the assumption that $u \ll c$. The CR current $\boldsymbol{j}_{\mathrm{CR}}$, required for insertion into the MHD momentum equation, is calculated by integration over f in momentum space. The magnetic field in the CR kinetic equation is taken from the MHD calculation.

As in Lucek & Bell (2000) and Bell (2004) three spatial dimensions are needed to represent the turbulence adequately. Since our aim is to investigate the mutual interactions of magnetic field amplification, CR acceleration and CR escape upstream of the shock, we need to model the complete system including the shock and the complete CR precursor. Because we model the detailed interaction between the CR and the distorted magnetic field, we need to resolve the CR Larmor radius in configuration space and the rotation of CR trajectories in momentum space. As a consequence, the numerical model should be 6D in momentum-configuration space with spatial scales extending from the CR Larmor radius of the lowest energy CR

to the precursor scaleheight of the highest energy CR. This would be impossible without extraordinary computational resources so our strategy is to design a computational model that includes all the important processes at a minimal level. We retain the three dimensions in configuration space but limit the range of CR momentum to a factor of 10 so that we do not have to resolve the Larmor radius of very low energy CR. We choose a shock velocity $u_s = c/5$ to keep the ratio of the CR to the MHD time-scale to a minimum while staying close to the range of conceivable SNR expansion speeds. Our greatest approximations are made in the momentum space representation of the CR distribution function since this is the aspect of the calculation in which the number of dimensions can be reduced.

The VFP equation (equation 8) is important in the physics of laser-produced plasmas where it is solved in finite difference form to model electron transport. The successful use of the VFP simulation to model electron transport in laser-produced plasmas stretches back more than 30 years (Bell, Evans & Nicholas 1981) so it is natural to apply the techniques to CRs that obey the same equation. The distribution function $f(\boldsymbol{r}, \boldsymbol{p}, t)$ of charged particles (CRs or energetic electrons) is usually represented in spherical coordinates (p, θ, ϕ) in momentum space. A common representation of the distribution function is as a sum of spherical harmonics:

$$f(\boldsymbol{r}, \boldsymbol{p}, t) = \sum_{l,m} f_l^m(\boldsymbol{r}, p, t) P_l^{|m|}(\cos\theta) \mathrm{e}^{\mathrm{i}m\phi}, \quad l = 0, \infty, \quad m = -l, l, \quad f_l^{-m} = \left(f_l^m\right)^*, \tag{9}$$

where $f_l^m(\boldsymbol{r}, p, t)$ is the coefficient for the (l, m) spherical harmonic. $f_l^m(\boldsymbol{r}, p, t)$ is a function of time, position and magnitude of momentum p. The spherical harmonics describe the angular structure on shells of constant magnitude of momentum. Reviews of the VFP technique, or papers containing a significant review element, are Bell et al. (2006), Tzoufras et al. (2011) and Thomas et al. (2012). For information on the application of VFP techniques to CR acceleration, the reader is referred to Reville & Bell (2013) which includes an appendix setting out the full VFP equations for a spherical harmonic expansion. Bell, Schure & Reville (2011) also apply VFP techniques to CR acceleration. The use of an expansion in tensors (used here) as an alternative to spherical harmonics is discussed by Schure & Bell (2011).

VFP simulation was used by Bell, Schure & Reville (2011) for the calculation of CR acceleration by oblique shocks. They found that an expansion to the 15th harmonic could be needed for oblique shocks because of the abrupt change in magnetic field direction at the shock, but that only a few harmonics are needed for quasi-parallel shocks. Here we reduce the computational size of the problem by modelling parallel shocks in which the zeroth-order magnetic field is parallel to the shock normal. There are good reasons to suppose that the first few terms in the expansion capture the essential physics. First, as shown by Bell (2004), the NRH instability is driven by the CR current density $\boldsymbol{j}_{\mathrm{CR}}$. Higher order anisotropies do not directly contribute to the instability. Secondly, the CR precursor scaleheight is c/u_s times the CR scattering mean free path in standard DSA theory. DSA theory is based on the diffusive approximation in which only the first-order anisotropy is needed and only the first two terms (isotropy and drift anisotropy) in the harmonic expansion are retained. In diffusion theory, the higher order anisotropies are damped by scattering. Hence, it might be supposed that only the first two terms are needed and an adequate representation of the CR distribution function might be $f(\boldsymbol{r}, \boldsymbol{p}, t) = f_0^0(\boldsymbol{r}, p, t) + f_1^0(\boldsymbol{r}, p, t)\cos\theta + \Re\{f_1^1(\boldsymbol{r}, p, t)\sin\theta \mathrm{e}^{\mathrm{i}\phi}\}$. This '$f_0 + f_1$' expansion allows free CR propagation along magnetic field lines but restricts transport across the magnetic field because the direction of the anisotropic drift term is rotated by the field. However, this expansion omits an essential feature of CR transport. It does not allow CRs to gyrate as they travel along a magnetic field line. The $f_0 + f_1$ expansion allows CRs to propagate along field lines and separately it allows CRs to gyrate around field lines, but it does not allow CRs to do both at the same time. Spiral trajectories require the inclusion of the off-diagonal components of the stress tensor f_2. Without the stress tensor, CRs cannot resonantly interact in space with magnetic perturbations on the scale of a Larmor radius. Clearly this would rule out the Alfvén instability, and more surprising it also rules out the NRH instability. The role of the stress tensor is discussed by Schure & Bell (2011) in which the linear NRH dispersion relation is derived with the perturbed CR distribution expressed as a tensor expansion. We proceed on the basis that the CR distribution function may be adequately represented by an isotropic part (zeroth order in u_s/c) plus a drift component (first order in u_s/c) plus a term representing the stress tensor (second order in u_s/c). This second-order expansion is more easily represented in the equivalent tensor notation instead of spherical harmonics:

$$f(\boldsymbol{r}, \boldsymbol{p}, t) = f_0(\boldsymbol{r}, p, t) + f_i(\boldsymbol{r}, p, t)\frac{p_i}{p} + f_{ij}(\boldsymbol{r}, p, t)\frac{p_i p_j}{p^2}, \tag{10}$$

where the trace of f_{ij} is zero because it is already accounted for in the isotropic term f_0. Following Johnston (1960), the reduced Vlasov equation for the CR distribution function is then

$$\frac{\partial f_0}{\partial t} + \frac{\partial (f_0 u_i)}{\partial r_i} = -\frac{c}{3}\frac{\partial f_i}{\partial r_i} + \frac{\partial u_i}{\partial r_i}\frac{1}{3p^2}\frac{\partial (p^3 f_0)}{\partial p}, \tag{11a}$$

$$\frac{\partial f_i}{\partial t} + \frac{\partial (f_i u_j)}{\partial r_j} = -c\frac{\partial f_0}{\partial r_i} - \frac{2c}{5}\frac{\partial f_{ij}}{\partial r_j} - \epsilon_{ijk}\frac{ceB_j}{p} f_k, \tag{11b}$$

$$\frac{\partial f_{ij}}{\partial t} + \frac{\partial (f_{ij} u_k)}{\partial r_k} = -\frac{c}{2}\left(\frac{\partial f_i}{\partial r_j} + \frac{\partial f_j}{\partial r_i}\right) + \frac{c}{3}\delta_{ij}\frac{\partial f_k}{\partial r_k} - \frac{ceB_k}{p}\left(\epsilon_{kil} f_{lj} + \epsilon_{kjl} f_{li}\right), \tag{11c}$$

where quadratic-order terms in the velocity $\boldsymbol{u}$ have been neglected and we have omitted terms involving $\partial f/\partial p$ times a gradient of $\boldsymbol{u}$ apart from the term in equation (11a) for the evolution of f_0. This amounts to the neglect of second-order Fermi acceleration and the acceleration resulting from shear motions in the background hydrodynamics. In our problem, these processes are small in comparison with acceleration at the shock.

We have chosen to terminate the set of equations at equation (11c) by setting f_{ijk} to zero. Additionally, we soften the termination of the tensor expansion by replacing the magnetic rotation in equation (11c) by a damping term with a damping rate equal to the magnetic gyration frequency. The logic of this approximation is that random rotation of the stress tensor anisotropy leads to its damping. A similar assumption underlies Bohm diffusion which replaces rotation of f_i by a damping rate, thereby terminating the tensor expansion at f_i, whereas we terminate it at f_{ij}. Our approximation makes intuitive sense, and we support it in Appendices D and E by examining its effect on propagating modes and on the NRH instability.

The notation is simplified by introducing the vector g_i related to shear and vorticity ($\nabla \times \boldsymbol{f}_1$) in CR motion to represent the off-diagonal components of the stress tensor. The on-diagonal components of f_{ij} ($i = j$) are accounted for by multiplying the $-c\partial f_0/\partial r_i$ term in equation (11b) by 9/5 to allow for the stress tensor contribution to compressional waves and to allow freely streaming CRs

to propagate at $\sqrt{3/5}c$ instead of $\sqrt{1/3}c$, as shown in Appendix D. The equations to be solved (their derivation is given in Appendix C) are then

$$\begin{aligned}
&\frac{\partial f_0}{\partial t} + \frac{\partial (f_0 u_i)}{\partial r_i} = -\frac{c}{3}\frac{\partial f_i}{\partial r_i} + \frac{\partial u_i}{\partial r_i}\frac{1}{3p^2}\frac{\partial (p^3 f_0)}{\partial p}\,,\\
&\frac{\partial f_i}{\partial t} + \frac{\partial (f_i u_j)}{\partial r_j} = -\frac{9}{5}c\frac{\partial f_0}{\partial r_i} - \frac{1}{5}c\epsilon_{ijk}\frac{\partial g_k}{\partial r_j} - \epsilon_{ijk}\frac{ceB_j}{p}f_k\,,\\
&\frac{\partial g_i}{\partial t} + \frac{\partial (g_i u_j)}{\partial r_j} = c\epsilon_{ijk}\frac{\partial f_k}{\partial r_j} - \nu_B g_i\,.
\end{aligned} \tag{12}$$

Equivalently, expressed in vector notation,

$$\begin{aligned}
&\frac{\partial f_0}{\partial t} + \nabla\cdot(\boldsymbol{u} f_0) = -\frac{c}{3}\nabla\cdot\boldsymbol{f}_1 + \frac{\nabla.\boldsymbol{u}}{3p^2}\frac{\partial (p^3 f_0)}{\partial p}\,,\\
&\frac{\partial \boldsymbol{f}_1}{\partial t} + \nabla\cdot(\boldsymbol{u} f_1) = -\frac{9c}{5}\nabla f_0 - \frac{c}{5}\nabla\times\boldsymbol{g}_1 - \boldsymbol{\Omega}\times\boldsymbol{f}_1\,,\\
&\frac{\partial \boldsymbol{g}_1}{\partial t} + \nabla\cdot(\boldsymbol{u} g_1) = c\nabla\times\boldsymbol{f}_1 - \nu_B\boldsymbol{g}_1\,,
\end{aligned} \tag{13}$$

where $\boldsymbol{\Omega} = ec\boldsymbol{B}/p$ is the vector CR Larmor frequency and we take $\nu_B = ecB/p$. The presence of the curls of $\boldsymbol{f}_1$ and $\boldsymbol{g}_1$ facilitates the propagation of transverse modes in $\boldsymbol{f}_1$ and $\boldsymbol{g}_1$ as needed for helical motion along magnetic field lines or CR propagation at an angle to the wavevector $\boldsymbol{k}$.

The termination of the harmonic expansion at the stress tensor makes the computation tractable with available resources. Appendices D and E show that the truncated expansion provides an adequate representation of the essential physics of CR propagation and CR-driven instability.

5 THE SIMULATION

A full 3D simulation with realistic parameters is not possible because of the large ratio of the largest distances (the CR precursor scaleheight and the CR free-escape distance) to the smallest distance (the shortest wavelength on which the NRH instability grows). The correspondingly large ratio of the largest time-scale (the SNR expansion time) to the shortest time-scale (the shortest NRH growth time) similarly makes substantial demands on computer resources. The computational constraints are discussed in Appendix F.

We artificially increase the magnetic field and stretch other parameters in a favourable direction, choosing

$$\begin{aligned}
&n_e = 0.1\ \mathrm{cm}^{-3}\,, \quad u_s = 60\,000\ \mathrm{km\ s}^{-1}\,,\\
&B_0 = 47\ \mu\mathrm{G}\,, \quad v_A = 3\times10^5\ \mathrm{m\ s}^{-1}\,, \quad T_{\mathrm{inject}} = 100\ \mathrm{TeV}\,,
\end{aligned} \tag{14}$$

where T_{inject} is the energy at which CRs are injected at the shock. The zeroth-order magnetic field is aligned along the shock normal. The instability is seeded by imposing random fluctuations on the magnetic field with a mean magnitude of 9 μG. CRs are injected at the shock into the lowest momentum bin (width Δp) according to the rule

$$4\pi p^2\Delta p\, cp\frac{\partial f_0}{\partial t} = -\mathrm{constant}\times\nabla\cdot\boldsymbol{u}\ \min(\rho_0 u^2, U)\,, \tag{15}$$

where ρ_0 is the density upstream of the shock and u is the local background fluid velocity relative to the initially stationary upstream plasma. U is the local thermal energy density. This prescription is designed to inject a suitable energy density of CRs at the shock, dependent on the choice of the constant, whilst avoiding a negative value of U due to excessive transfer of energy to CRs from cold plasma at the foot of the shock. The resulting CR current density ahead of the shock is displayed in panel (e) of Figs 2 and 3. The peak CR current density in the population freely escaping ahead of the shock in Fig. 2 is

$$j_{\mathrm{CR}} = 1.1\times10^{-14}\ \mathrm{A\,m}^{-2}\,. \tag{16}$$

This current density corresponds to $\eta = 0.026$, giving

$$\gamma_{\mathrm{max}}^{-1} = 2.3\times10^6\ \mathrm{s}\,, \quad c\gamma_{\mathrm{max}}^{-1} = 7\times10^{14}\ \mathrm{m}\,, \tag{17}$$

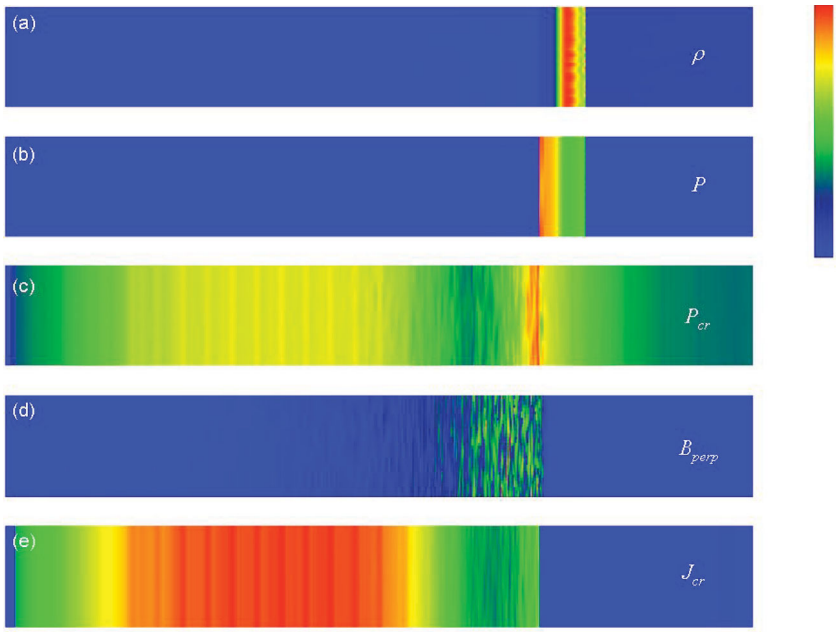

Figure 2. 2D slices of a 3D simulation with peak values in brackets: electron density (9.7 cm^{-3}), pressure (340 nPa), CR pressure (2.3 nPa), magnitude of the magnetic field perpendicular to the shock normal (610 μG), CR current parallel to the shock normal (1.1×10^{-14} $\mathrm{A\,m}^{-2}$). $t = 4.12\times10^7$ s (1.3 yr). The dimensions of the computational box are 7.9×10^{15} m by 4.5×10^{13} m. The horizontal spatial scale, in the direction of the shock normal, is artificially compressed by a factor of 24.

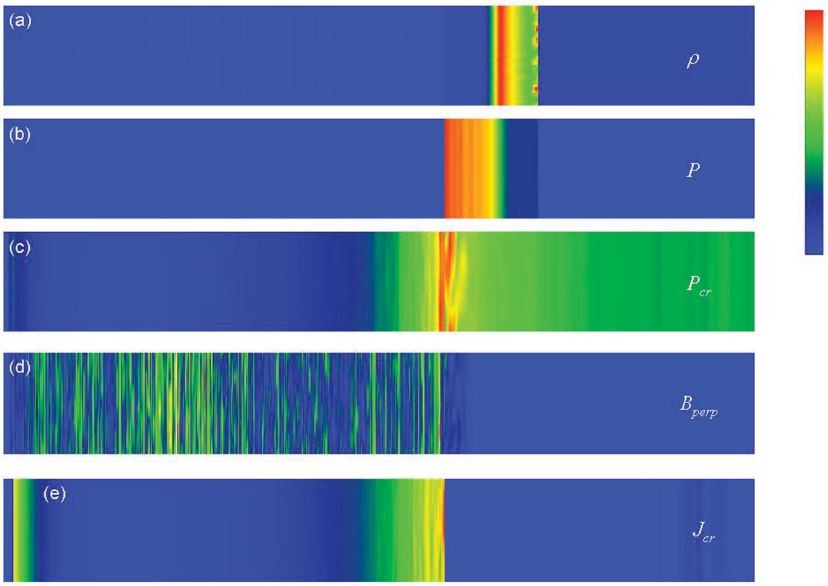

Figure 3. 2D slices of a 3D simulation with peak values in brackets: electron density ($6.9\,\mathrm{cm}^{-3}$), pressure (320 nPa), CR pressure (1.9 nPa), magnitude of the magnetic field perpendicular to the shock normal (590 μG), CR current parallel to the shock normal ($4.2 \times 10^{-15}\,\mathrm{A\,m}^{-2}$). $t = 6.18 \times 10^7$ s (2.0 yr). The dimensions of the computational box are 7.9×10^{15} m by 4.5×10^{13} m. The horizontal spatial scale, in the direction of the shock normal, is artificially compressed by a factor of 24.

$$k_{\mathrm{max}}^{-1} = 7 \times 10^{11}\,\mathrm{m}\,, \quad r_{\mathrm{g}} = 7 \times 10^{13}\,\mathrm{m}\,,$$
$$r_{\mathrm{g}} k_{\mathrm{max}} = 100\,, \quad M_{\mathrm{A}} = 200\,. \tag{18}$$

We use a spatial grid with $\Delta x = \Delta y = \Delta z = 1.4 \times 10^{12}$ m. 10 cells in momentum cover an energy range from 100 TeV to 1 PeV with logarithmic spacing. There are 32 cells in each of x and y with periodic boundary conditions. In contrast, 5676 cells are used in z with reflective boundary conditions for the MHD part of the code and for CRs at the right-hand boundary. CRs reaching the left-hand boundary are disposed of on the assumption that they escape freely. Correspondingly, the computational box extends 7.9×10^{15} m by 4.5×10^{13} m by 4.5×10^{13} m. The box-size in x and y is comparable with the initial CR Larmor radius, but the Larmor radius contracts significantly as the magnetic field is amplified. The cell-size is π^{-1} times the wavelength of the fastest growing mode, which is barely sufficient to represent the initial growth of the instability, but the characteristic scalelength of the instability increases rapidly as its amplitude grows. These parameters are only marginally sufficient to represent the physics, but, for example, a halving of the computational cell-size would increase the computational cost by a factor of 16. The simulation in Fig. 3 was run for 6.2×10^7 s = 2 yr using 128 processors for 75 h on the SCARF-LEXICON cluster at the UK Rutherford Appleton Laboratory. The MHD part of the code is the same as that used by Lucek & Bell (2000) and Bell (2004). The VFP part of the code that models the CR uses a second-order Runge–Kutta scheme in configuration space, a donor-cell scheme in magnitude of momentum, and the Boris algorithm for rotation in momentum due to magnetic field as used in particle-in-cell codes (Birdsall & Langdon 1985). The VFP equations are formulated in tensor notation rather than in spherical harmonics, but the two formulations are similar for the low-order expansion used here, and their numerical solution is informed by experience with the KALOS spherical harmonic code (Bell et al. 2006) where Runge–Kutta advection is found to be robust, sufficiently accurate, and a good fit to the form of the equations. Numerical diffusion due to limited spatial resolution is ameliorated by designing the simulation to initialize the upstream background plasma at rest relative to the computational grid. The more usual approach of initiating the simulation by setting the background plasma in motion towards a reflective boundary would exacerbate the effect of numerical diffusion on small structures during advection. Instead, a dense piston is initialized moving leftwards from the right-hand boundary, pushing a shock before it into the stationary background plasma.

6 SIMULATION RESULTS IN 3D

Results from the 3D simulation are presented in Figs 2 and 3 at $t = 4.1 \times 10^7$ and 6.2×10^7 s, respectively. Note that the horizontal spatial scales, in the direction of the shock normal, are artificially compressed by a factor of 24. The actual aspect ratio of the computational box is 177:1. The plot of the background plasma density in panel (a) shows the position of the dense plasma piston propagating leftwards and pushing the shock ahead of it. The high-pressure region in panel (b) is due to plasma heating at the shock. The CR pressure is plotted in panel (c). The maximum CR pressure occurs at the shock. Panel (c) of Fig. 2 shows the CR population dividing into a population freely propagating ahead of the shock and a population confined by magnetic field (panel d) near the shock. CRs confined near the shock continue to be accelerated. The banded structure in the CR pressure ahead of the shock in panel (c) is exaggerated by the colour coding. It represents only a variation of a few per cent in the CR pressure and probably arises from a small oscillation in the injection rate at the shock. Also, the horizontal spatial compression of Fig. 2 distorts the aspect ratio of the bands.

The escaping CRs are an essential aspect of the process of CR confinement by the self-generated magnetic field. They excite the instability and carry the escaping areal charge $Q_{\mathrm{CR}} = \int j_{\mathrm{CR}} \mathrm{d}t$ identified in equation (1) as necessary for substantial field amplification. In Fig. 2, the escaping CRs are only just reaching the left-hand side of the grid where the integral $\int j_{\mathrm{CR}} \mathrm{d}t$ is small and

field amplification is negligible. In contrast, immediately in front of the shock in Fig. 2 $\int j_{\rm CR} {\rm d}t$ has reached the critical value needed for strong field amplification causing the onset of CR confinement.

By the time of Fig. 3 most of the escaping population has passed through the free-escape boundary at the left-hand end of the grid. By this time, a large magnetic field in the upstream plasma has switched off CR escape, creating an expanse of low CR density between the confined and escaping CR populations. Panel (d) shows that the magnetic field is amplified by an order of magnitude by the escaping CRs over a large distance ahead of the shock.

The separation of CRs into escaping and confined populations matches expectations from the argument in Section 3. The CR charge per unit shock area in the escaping population is $\sim 1 \times 10^{-7}$ coulomb m^{-2} in Fig. 2 in good agreement with the estimate of 1.3×10^{-7} coulomb m^{-2} from equation (1). Panels (e) in Figs 2 and 3 plot the CR current density ahead of the shock.

7 SIMULATION RESULTS IN 2D

Fig. 4 follows the calculations of Figs 2 and 3 to later times with the same parameters but in 2D instead of 3D to reduce the demand on computer resources. The top row of plots in Fig. 4 is the 2D equivalent of the 3D results in Fig. 2 at $t = 4.1 \times 10^7$ s. The dimensions of the spatial grid are the same as in Fig. 2 and the top row of Fig. 4. In subsequent rows of Fig. 4, the spatial dimensions normal to the shock are expanded by factors of 2, 3 and 4 such that CRs travel the length of the grid in the respective times ($t = 8.2 \times 10^7$, 1.2×10^8 and 1.6×10^8 s).

In 3D at $t = 4.1 \times 10^7$ s the dip in the CR density separating the escaping and confined CRs has only recently formed as shown in Fig. 2(c). At the same time in 2D (Fig. 4, top row), the separation between the confined and escaping populations is relatively more developed. Otherwise, the results are similar in 2D and 3D. The reason for the slightly earlier development of CR confinement in Fig. 4 is that magnetic structures can expand more freely in 2D. In 2D, magnetic structures expand in the ignored dimension without running into stationary or counterpropagating plasma. Non-linear development in 2D is therefore less inhibited and the magnetic field grows more rapidly. The magnetic field in 2D reaches a steady value similar to that found in the 3D calculation. The eventual limit on the magnitude of the magnetic field may be set by magnetic tension which operates equally in 2D and 3D.

Comparison of the CR distributions at different times in Fig. 4 shows that at early times ($t = 4.1 \times 10^7$ s) only the low-energy CRs are confined. At $t = 8.2 \times 10^7$ s, CRs are confined at 100 and 167 TeV with the confinement beginning to occur at 278 TeV

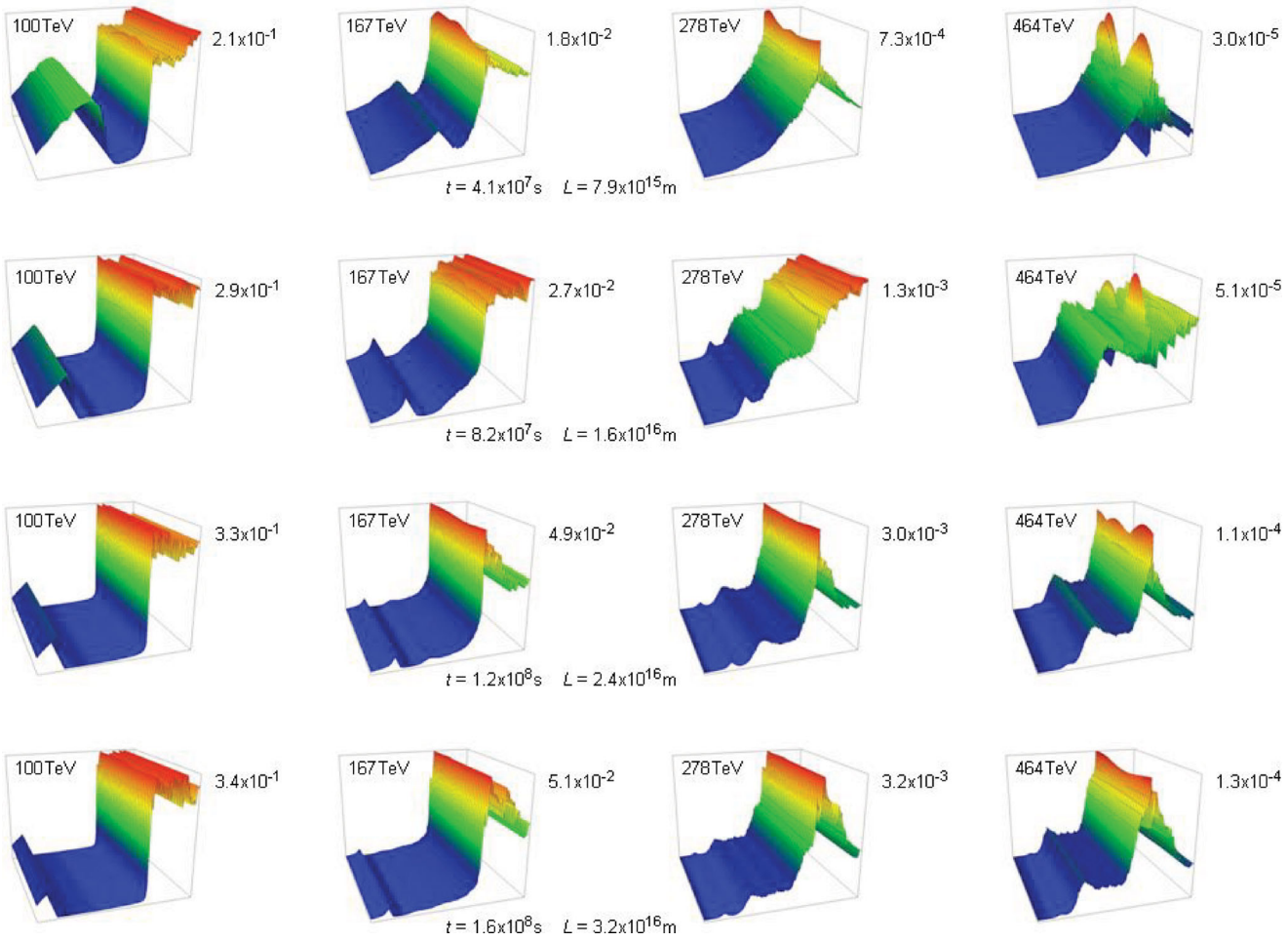

Figure 4. 2D simulations. Plots of $f_0 p^3$ at CR energies 100, 167, 278 and 464 TeV at times between 4.1×10^7 s (top row) and 16×10^7 s (bottom row), with computational box lengths L proportional to t between 7.9×10^{15} and 3.2×10^{16} m chosen such that the CRs travel the length of the box during the simulation time. The width of the computational box is 4.5×10^{13} m in each plot. The vertical axes are in dimensionless units with peak values given against the axis.

and no evidence of the development of two separate populations in the few CRs reaching 464 TeV. By $t = 1.2 \times 10^8$ s a larger number of CRs have reached 464 TeV with a local minimum in CR density $f_0 p^3$ evident at all energies up to 464 TeV in front of the shock. By $t = 1.2 \times 10^8$ s, CRs at 100 and 167 TeV are strongly confined with a short precursor scaleheight ahead of the shock, which is unsurprising since the Larmor radius of a 100 TeV proton in a 700 μG magnetic field is 5×10^{12} m. By $t = 1.6 \times 10^8$ s CRs are confined at all energies up to 464 TeV.

At all four times in Fig. 4, the CR spectrum is much steeper than the steady-state test particle spectrum ($f_0 \propto p^{-4}$) because of CR loss into the downstream plasma. Magnetic field amplification takes place ahead of the shock and the downstream field only becomes large when the shock overtakes the field amplified in the upstream. Hence, at early times CRs escape downstream. This causes a reduction in the number of CRs accelerated to high energy at the shock, thereby steepening the spectrum. Downstream confinement at the shock improves at later times as shown by the downstream gradients in f_0 at $t = 1.2 \times 10^8$ and 1.6×10^8 s. However, unphysical numerical relaxation of the spatially compressed downstream magnetic field due to limited spatial resolution may be playing a part in allowing CRs to escape downstream.

There is slight evidence of pulsed acceleration as seen in the three separate peaks in the 278 TeV CR density at $t = 1.2 \times 10^8$ and 1.6×10^8 s, but overall the CR profiles develop in an orderly manner.

8 APPLICATION TO SNRs

Our simulations support the model developed in Section 3. According to our model, CRs are confined and accelerated if the electrical charge of CRs escaping upstream of the shock reaches $Q_{\rm CR} = 10\sqrt{\rho/\mu_0}$ coulomb m^{-2}. We now apply this to spherical SNR shocks. The CR current density at a radius R is $j_{\rm CR} = \eta\rho u_{\rm s}^3 r^2/R^2 T$ due to CRs accelerated to energy eT when the shock radius was r. Since only the highest energy CRs escape upstream, we assume that the CRs reaching the radius R are monoenergetic with energy eT. T evolves as the shock expands. When the SNR shock reaches the radius R, CRs are confined if

$$\int_0^R \frac{\eta\rho(r)u_{\rm s}^2(r)}{T(r)}\, r^2 {\rm d}r = 10R^2\sqrt{\frac{\rho(R)}{\mu_0}}\,. \tag{19}$$

Differentiating this equation with respect to R and assuming a power-law dependence of density on radius, $\rho(R) = \rho_0(R/R_0)^{-m}$,

$$T(R) = \frac{\eta\sqrt{\mu_0}}{5(4-m)} u_{\rm s}^2 R\sqrt{\rho}\,. \tag{20}$$

Defining $u_7 = u_{\rm s}/10\,000$ km s^{-1}, $R_{\rm pc} = R/{\rm pc}$, $\eta_{0.03} = \eta/0.03$, $n_{\rm e} = \rho/2 \times 10^{-21}$ kg cm^{-3} (such that $n_{\rm e}$ is approximately the electron density in cm^{-3}), and taking $m = 0$ for expansion into a uniform medium,

$$T = 230\eta_{0.03} n_{\rm e}^{1/2} u_7^2 R_{\rm pc}\ {\rm TeV}\,. \tag{21}$$

A SNR with $u_7 = 0.6$, $n_{\rm e} = 1$ and $R_{\rm pc} = 1.7$, representative of Cas A, would then accelerate CRs to ∼140 TeV. A SNR with $u_7 = 0.5$, $n_{\rm e} = 0.1$ and $R_{\rm pc} = 10$, representative of SN1006, would accelerate CRs to ∼180 TeV. These energies are a factor of 10 lower than the energy of the knee. Abbasi et al. (2013) place the knee at 4–5 PeV, although data from other experiments indicate a lower energy and the turnover in the spectrum is not well defined as shown in their fig. 15.

Our model places a considerable question mark over the ability of the well-known historical SNRs to accelerate CRs to the knee. Acceleration by SNRs such as Cas A and SN1006 fails to reach the knee in our analysis because their expansion is already significantly decelerated. Zirakashvili & Ptuskin (2008) also reach the conclusion (their table 2) that the historical SNRs do not accelerate CRs beyond 100–200 TeV, but note that their parameter $\eta_{\rm esc}$ differs from our parameter η by a factor of 2 ($\eta_{\rm esc} = 2\eta$).

Initial expansion velocities of very young SNRs can reach 30 000 km s^{-1} (Manchester et al. 2002) or possibly higher for some types of SNe (Chevalier & Fransson 2006). According to equation (21) expansion into a density of 1 cm^{-3} at 30 000 km s^{-1} for 16 yr to a shock radius of 0.5 pc accelerates CRs to ∼1 PeV. Moreover, the energy processed through the shock is comparable to that for expansion to 1.5 pc at 6000 km s^{-1}, thereby contributing a comparable CR energy content to the Galactic energy budget. A complementary perspective on the same problem is obtained by expressing the maximum CR energy in terms of the mass $M = 4\pi\rho R^3/3$ swept up by the shock and the characteristic energy of the blast wave $E = Mu_{\rm s}^2/2$. If $\mathrm{M}_\odot$ is the mass in units of a solar mass and E_{44} is the energy in units of 10^{44} J, the maximum CR energy is

$$T = 0.5\eta_{0.03} n_{\rm e}^{1/6} E_{44}\, \mathrm{M}_\odot^{-2/3}\ {\rm PeV}\,, \tag{22}$$

which indicates that a typical SNR should be able to accelerate CRs to ∼1 PeV and that the maximum CR energy is greater for the same energy E given to a smaller mass M. The maximum CR energy is nearly independent of density $n_{\rm e}$ because a shock expands to a larger radius in a low-density medium before deceleration (Hillas 2006).

In the self-similar Sedov phase, E is constant, M is proportion to R^3 and hence $T \propto R^{-2}$. The maximum CR energy decreases with radius during the Sedov phase until magnetic field amplification ceases, at which point our analysis in terms of the charge carried by escaping CRs is inapplicable.

Equation (20) with $m = 2$ indicates that the highest CR energies might be achieved by SNR shocks expanding into a dense circumstellar medium previously ejected as a wind from the SN progenitor. ρR^2 is independent of radius in a steady wind, in which case the CR energy depends only on $u_{\rm s}^2$ and η according to equation (20), thus favouring CR acceleration in the very early stages of rapid expansion as previously suggested by Völk & Biermann (1988) and Bell & Lucek (2001). The maximum CR energy for a SNR expanding into a wind carrying $\dot{M}_5 \times 10^{-5}$ $\mathrm{M}_\odot$ yr^{-1} at a velocity of $v_4 \times 10$ km s^{-1} is

$$T = 760\eta_{0.03} u_7^2 \sqrt{\frac{\dot{M}_5}{v_4}}\ {\rm TeV} \tag{23}$$

indicating that PeV energies are attainable. CRs may be accelerated to energies beyond the knee if the initial shock velocity is ∼30 000 km s^{-1} and the shock expands into a particularly dense wind or otherwise dense circumstellar medium.

The estimates made in this section are subject to considerable numerical uncertainty. For example, our estimates for the efficiency $\eta \sim 0.03$ or the escaping charge $Q_{\rm CR} = 10\sqrt{\rho/\mu_0}$ could be uncertain by a factor of 2 or 3. However, the accumulated error in our estimates would need to be a factor of 10 for the well-known historical SNR to account for acceleration to the knee. Our arguments are not completely watertight but we tentatively conclude that acceleration to the knee takes place in younger relatively undecelerated SNRs.

9 THE CR ENERGY SPECTRUM

In this section, we discuss the energy spectrum of escaping CRs integrated over the lifetime of the SNR. The energy T of escaping CRs changes as the SNR evolves in radius and expansion velocity. The integrated energy spectrum of CRs escaping into the ISM need not be the same as the spectra of CRs at the shock during acceleration or that of CRs carried downstream into the interior of the SNR. Related analyses based on different models of CR escape can be found in Caprioli et al. (2010a), Drury (2011), Ohira et al. (2010), Ptuskin & Zirakashvili (2003) and Ptuskin et al. (2010).

We assume a power-law density gradient, $\rho \propto R^{-m}$, where $m = 0$ for a uniform circumstellar medium and $m = 2$ for a steady pre-SN wind. We further assume that the shock velocity can be approximated as a power law $u_\mathrm{s} \propto R^{-q}$ over a sufficiently large part of the SNR's evolution. In this approximation, $u_\mathrm{s} \propto t^{-q/(1+q)}$ and $R \propto t^{1/(1+q)}$. In the Sedov phase, $q = 3/2$. From equation (20), $T \propto R^{1-2q-m/2}$.

In a uniform circumstellar medium ($m = 0$), the energy T of escaping CRs decreases during expansion if $q > 1/2$, which is equivalent to u_s decreasing more rapidly than $t^{-1/3}$. If a SNR expands into a steady pre-SN wind ($m = 2$), the maximum CR energy always decreases with time, provided u_s decreases with time ($q > 0$) as expected.

Let $\int_T^\infty E(T)\,\mathrm{d}T$ be the total energy given to CRs above an energy T. By definition of η the CR energy flux escaping upstream is $\eta\rho u_\mathrm{s}^3$, so $\int_T^\infty E(T)\,\mathrm{d}T = \int_0^R \eta 4\pi r^2 \rho u_\mathrm{s}^2\,\mathrm{d}r$ and

$$E = -\frac{\mathrm{d}R}{\mathrm{d}T}\,\eta 4\pi R^2 \rho u_\mathrm{s}^2, \tag{24}$$

where CRs with energy T escape when the shock radius is R. From equation (20)

$$\frac{T}{T_0} = \left(\frac{R}{R_0}\right)^{1-2q-m/2}, \text{ where } T_0 = \frac{\eta\sqrt{\mu_0}}{5(4-m)} u_0^2 R_0 \sqrt{\rho_0}, \tag{25}$$

and ρ_0, u_0 and T_0 are the values of ρ, u_s and T at a reference radius $R = R_0$. Manipulating these equations gives

$$N_\mathrm{CR} = \frac{4\pi\eta\rho_0 u_0^2 R_0^3}{(2q - 1 + m/2) e T_0^2}\left(\frac{T}{T_0}\right)^{-\alpha},$$
$$\text{where} \quad \alpha = \frac{4q+2}{4q+m-2} \tag{26}$$

and $N_\mathrm{CR}(T) = E/eT$ is the CR differential spectrum in energy. For SNR expansion into a uniform medium, the CR spectral index is $\alpha_\mathrm{uniform} = (2q + 1)/(2q - 1)$, and for expansion into a wind the index is $\alpha_\mathrm{wind} = (2q + 1)/2q$. During the Sedov phase, $m = 0$ and $q = 3/2$, giving

$$\alpha_\mathrm{Sedov} = 2 \tag{27}$$

although the analysis only applies while the magnetic field is being amplified by the NRH instability. A slightly less rapid decrease in shock velocity, $u_\mathrm{s} \propto t^{-0.57}$ ($q = 4/3$), would reproduce the CR spectral index ($\alpha \approx 2.2$) inferred for CRs at their source at energies less than 1 PeV (Gaisser, Protheroe & Stanev 1998; Hillas 2005). The spectral index of CRs escaping in the Sedov phase, $\alpha_\mathrm{Sedov} = 2$, is the same as that for test particle acceleration at a strong shock. There is no obvious reason why this should be so.

We emphasize that this discussion and the derived spectral index α or α_Sedov applies only to CRs escaping upstream from the shock during SNR expansion. A further population of lower energy CRs is carried into the centre of the SNR where they reside until they are released into the ISM when the SNR slows, disintegrates and dissolves into its surroundings. These lower energy particles lose energy adiabatically as the SNR expands but they can be expected to contribute most of the Galactic population of low-energy CRs.

In Section 8, we suggested that acceleration beyond the knee might result from high-velocity expansion into a dense circumstellar medium. The CR population beyond 1 PeV is an uncertain mix of protons and heavy ions. The overall spectral index of CRs released into the Galaxy by SNRs beyond 1 PeV can be approximated as $\alpha \approx 2.7$ with further spectral steepening occurring during propagation from the source to the Earth. This spectral index at source is predicted by our analysis if $q = 0.29$ ($u_\mathrm{s} \propto t^{-0.22}$) for expansion into a steady wind. It would correspond to a reduction in the shock velocity by a quite reasonable factor of 2.1 between $t = 10$ and 300 yr. Expansion into a uniform medium would require $q = 1.09$ ($u_\mathrm{s} \propto t^{-0.52}$) equivalent to a reduction in shock velocity by a less reasonable, but not impossible, factor of 5.9 between $t = 10$ and 300 yr. This supports the contention that acceleration to 10–100 PeV may occur at a SNR shock expanding into a circumstellar wind.

10 MAGNETIC FIELD

The Hillas parameter $\xi u_\mathrm{s} BR$ (shock velocity times magnetic field times spatial scale) provides an estimate of the energy T_max to which CRs can be accelerated under various circumstances (Hillas 1984). ξ is a numerical factor of order unity, probably lying in the range between 1/8 and 3/8 depending upon the CR diffusion coefficient (Lagage & Cesarsky 1983a,b; Bell 2012). $T_\mathrm{max} = 4\xi_8 u_7 B_{\mu\mathrm{G}} R_\mathrm{pc}\,\mathrm{TeV}$, where $\xi = \xi_8/8$ ($\xi_8 = 1$ for $\xi = 1/8$). Combining this with equation (21) gives an estimate of the pre-shock magnetic field required to accelerate CRs to T_max:

$$B \sim 60\eta_{0.03}\xi_8^{-1} n_\mathrm{e}^{1/2} u_7\ \mu\mathrm{G}. \tag{28}$$

The post-shock field is approximately three times larger due to compression at the shock. For our simulation parameters ($n_\mathrm{e} = 0.1$, $u_7 = 6$), the estimated post-shock maximum magnetic field is $\sim$400 μG which is consistent with a field of $\sim$600 μG seen in panel (d) of Figs 2 and 3. This confirms that the magnetic field in the simulation is amplified sufficiently to confine and accelerate CRs and that diffusion in the CR precursor is approximately Bohm, $D \sim r_\mathrm{g} c$.

The above estimate of the magnetic field is derived on the basis that the magnetic field must be sufficient to contain and accelerate CRs to the energy estimated in equation (21). Continued growth in the magnetic field would inhibit CR escape and remove the CR current that drives the NRH instability. Part of the energy generated by the NRH instability is stored in the kinetic energy of plasma motions. These motions might continue to stretch magnetic field lines and further increase the magnetic field after the CR current becomes inhibited. Further release of CRs into the upstream plasma would then be heavily restricted until the magnetic field relaxes to a lower level. This might result in oscillation about a marginal state defined by a balance between magnetic field amplification and CR escape upstream. Weak evidence for periodic releases of CRs into the upstream plasma can be found in the plot of the 278 TeV CR density at 1.2×10^8 s in Fig. 4, but on the whole the system appears to evolve without oscillation.

In planar geometry, escaping CRs are in principle capable of generating magnetic field at an unlimited distance ahead of the shock. In the spherical geometry of an expanding SNR, the CR current decreases with distance ahead of the shock, $\boldsymbol{j}_\mathrm{CR} \propto R^{-2}$, so continuous CR escape is needed to amplify the magnetic field at a general radius R before the shock reaches that point. Hence, the

marginal balance between CR escape and magnetic field generation is more likely in spherical than planar geometry.

The above discussion assumes that magnetic field growth and CR acceleration are determined by the growth rate of the NRH instability. However, it is possible that the instability might saturate and stop growing before it reaches that given by equation (28). Bell (2004, 2009) argue that tension in the field lines limits amplification when $\nabla \times \boldsymbol{B} \sim \mu_0 \boldsymbol{j}_{\rm CR}$ for magnetic field structured on the scale of a CR Larmor radius. This implies a saturation magnetic energy density $B_{\rm sat}^2/\mu_0 \sim j_{\rm CR} T/c$ and predicts a saturated upstream magnetic field

$$B_{\rm sat} \sim 160\ \eta_{0.03}^{1/2} n_{\rm e}^{1/2} u_7^{3/2}\ \mu{\rm G} \tag{29}$$

with a further approximately three times increase at the shock. The ratio of the magnetic field given by equation (28) to the saturated magnetic field is

$$\frac{B}{B_{\rm sat}} \sim 0.4 \xi_8^{-1} \eta_{0.03}^{1/2} u_7^{-1/2}, \tag{30}$$

which implies that tension in the magnetic field does not stop the field growing to that given in equation (28). However, it would not require magnetic field growth to overshoot that indicated by equation (28) by a large factor before the magnetic tension intervenes to halt growth. According to equation (28) the magnetic energy density is proportional to $\rho u_{\rm s}^2$, whereas the magnetic energy density determined by saturation is proportional to $\rho u_{\rm s}^3$. Observations of SNRs slightly favour a dependence on $\rho u_{\rm s}^3$, but the difference is too close to be called (Vink 2006).

From equation (20) [$T = 0.05 \eta u_{\rm s}^2 R (\rho \mu_0)^{1/2}$ for $m = 0$] and the modified Hillas condition ($T = u_{\rm s} BR/8$), the required post-shock magnetic energy density is

$$\frac{B^2}{2\mu_0} \sim \eta^2 \rho u_{\rm s}^2. \tag{31}$$

For magnetic field structured on the scale of the Larmor radius of the highest energy CR, we should assume $\eta \sim 0.03$ as the fraction of $\rho u_{\rm s}^2$ given to the highest energy CR in which case the post-shock magnetic energy density would be ∼0.1 per cent of $\rho u_{\rm s}^2$, allowing for compression at the shock. Völk et al. (2005) find observationally that the post-shock magnetic energy density is typically ∼3 per cent of $\rho u_{\rm s}^2$ in the historical SNR. However, magnetic field will also be amplified on the scale of the Larmor radii of low-energy as well as high-energy CRs. The difference between ∼0.1 and ∼3 per cent may be explained by integration over the magnetic structures on scales varying by six orders of magnitude corresponding to the difference between the Larmor radii of GeV and PeV protons. If this is the case, most of the magnetic energy at the shock resides at scalelengths too short to accelerate CRs to PeV energies. The magnetic field inferred from X-ray synchrotron observations of a SNR shock should not be inserted without adjustment into the Hillas parameter to estimate the maximum CR energy.

Our analysis of CR escape leads to the result that the energy density of the magnetic field confining the highest energy CR is proportional to $\rho u_{\rm s}^2$. Previous analyses of CR escape often start from the assumption that the magnetic energy density is proportional to $\rho u_{\rm s}^2$ and consequently they produce similar results for the spectrum of escaping CRs. Comparable results for the CR spectrum produced in the Sedov phase can be found in Caprioli et al. (2010a), Drury (2011), Ohira et al. (2010), Ptuskin & Zirakashvili (2003) and Ptuskin et al. (2010). For example, a T^{-2} energy spectrum for escaping CRs in the Sedov phase has previously been derived by Berezhko & Krymskii (1988), Ptuskin & Zirakashvili (2005), Caprioli et al. (2010a) and Drury (2011).

11 CR ENERGY INPUT TO THE GALAXY

In our model, only the highest energy CRs escape upstream of the shock. At any given time, more CR energy is carried away downstream into the SNR than escapes into the Galaxy. Efficient production of Galactic CRs might therefore seem impossible. However, the CR energy carried into the interior of the SNR is subsequently recycled to drive the SNR expansion and is available to accelerate further CRs at a later stage. The overall efficiency of the production of Galactic CRs is demonstrated by integrating over the lifetime of the SNR. Assuming a T^{-2} energy spectrum ($\alpha = 2$, $q = 3/2$), equation (26) can be integrated to deduce a total CR energy input to the Galaxy:

$$E_{\rm total} = \frac{3\eta}{2} \frac{4\pi R_0^3}{3} \rho_0 u_0^2 \ln\left(\frac{T_2}{T_1}\right) \tag{32}$$

between energies T_1 and T_2 (∼1 GeV and ∼ 1 PeV, respectively). A small value of η (∼0.03) is balanced by the factor $\ln(T_2/T_1)$ which results from recycling CR energy carried into the interior of the SNR.

It is occasionally remarked that CR acceleration by very young SNRs during the first few years cannot inject sufficient energy into the Galaxy to account for CRs at energies beyond the knee because the SNR shock is small. However, if the CR spectrum connects smoothly across the knee and the spectrum beyond the knee of escaping CRs matches observation as shown to be possible in Section 9, then it follows that the CR energy input is sufficient to match the Galactic energy budget.

12 CONCLUSIONS

The central message of this paper is that CRs of a given energy escape freely ahead of a shock until magnetic field amplification takes place to inhibit propagation. The condition for propagation inhibition is that a sufficient number of CRs must escape upstream for the NRH instability to grow through ∼5–10 e-foldings at the growth rate of the fastest growing mode. Since the instability is driven by the CR current, the condition is that a CR electric charge $Q_{\rm CR} \sim 10\sqrt{\rho/\mu_0}$ per unit area must escape through a spherical surface surrounding the SNR to amplify the magnetic field and inhibit CR escape through that surface. Since high-energy CRs carry less charge than low-energy CRs for a fixed CR energy flux, the condition on $Q_{\rm CR}$ determines the energy of escaping CRs. We find that the energy eT of escaping CRs is proportional to $\eta R u_{\rm s}^2 \sqrt{\rho}$ as given by equation (21). The energy eT varies during the evolution of the SNR and determines the energy spectrum of CRs injected into the ISM by the SNR. In our estimation, the historical SNRs (Cas A, Tycho, Kepler, SN1006) are currently accelerating CRs to ∼100–200 TeV. Acceleration to the knee at a few PeV takes place in SNRs at an earlier stage of evolution when the shock velocity is ∼10 000 km s^{-1} or greater. This is an unsurprising conclusion since if the historical SNR were to accelerate CRs to the knee, we would be asking why even higher energy CRs were not being produced by younger SNRs. Observations by the planned Cherenkov Telescope Array should be crucial in testing our conclusions (Hinton & Hofmann 2010; Aharonian 2012).

Acceleration beyond the knee may take place in very young SNRs expanding at 20–30 000 km s^{-1} into a dense circumstellar pre-SN wind.

The spectral index of escaping CRs is consistent with the measured Galactic CR spectrum at energies less than 1 PeV. Beyond the knee the proton spectral index is uncertain both theoretically and observationally. The theoretical prediction depends on the rate at which the SNR shock decelerates during its early expansion.

The magnetic field can be estimated from the Hillas parameter as the field needed to accelerate CRs to the escape energy. The field is close to, but slightly less than, the saturation field determined by tension in the magnetic field. The predicted magnetic fields are consistent with those observed in SNRs if allowance is made for the large range of scalelengths, corresponding to the range of CR Larmor radii, in the structure of the magnetic field.

The model is tested against numerical simulations. The MHD/VFP code is 3D in space and 1D in CR momentum with anisotropy included to second order. The computational parameters are pushed to their limit to allow for a solution of this multiscale multidimensional problem, but the results support the analytic model. In the simulation, CRs are seen to escape upstream with the electrical charge predicted by theory and magnetic field is strongly amplified to the predicted level.

ACKNOWLEDGEMENTS

The research leading to these results has received funding from the European Research Council under the European Community's Seventh Framework Programme (FP7/2007-2013)/ERC grant agreement number 247039 and from grant number ST/H001948/1 made by the UK Science Technology and Facilities Council (STFC). We thank the STFC's e-Science facility for access to the SCARF computing cluster. We thank an anonymous referee for comments that considerably improved the presentation of this paper.

REFERENCES

Abbasi R. et al. (IceCube Collaboration), 2013, Astropart. Phys., 42, 15
Aharonian F. A., 2012, Astropart. Phys., doi: 10.1016/j.astropartphys.2012.08.007
Axford W. I., Leer E., Skadron G., 1977, Proc 15th Int. Cosmic Ray Conf. (Plovdiv), 11, 132
Bell A. R., 1978, MNRAS, 182, 147
Bell A. R., 2004, MNRAS, 353, 550
Bell A. R., 2005, MNRAS, 358, 181
Bell A. R., 2009, Plasma Phys. Control. Fusion, 51, 124004
Bell A. R., 2012, Astropart. Phys., doi: 10.1016/j.astropartphys.2012.05.022
Bell A. R., Lucek S. G., 2001, MNRAS, 321, 433
Bell A. R., Evans R. G., Nicholas D. J., 1981, Phys. Rev. Lett., 46, 243
Bell A. R., Robinson A. P. L., Sherlock M., Kingham R. J., Rozmus W., 2006, Plasma Phys. Control. Fusion, 48, R37
Bell A. R., Schure K. M., Reville B., 2011, MNRAS, 418, 1208
Berezhko E. G., Ellison D. C., 1999, ApJ, 526, L385
Berezhko E. G., Krymskii G. F., 1988, Sov. Phys. Usp., 31, 27
Berezhko E. G., Ksenofontov L. T., Völk H. J., 2003, A&A, 412, L11
Birdsall C. K., Langdon A. B., 1985, Plasma Physics via Computer Simulation. McGraw Hill, Singapore
Blandford R. D., Ostriker J. P., 1978, ApJ, 221, L29
Bykov A. M., Osipov S. M., Ellison D. C., 2011, MNRAS, 410, 39
Caprioli D., Blasi P., Amato E., 2009a, MNRAS, 396, 2065
Caprioli D., Blasi P., Amato E., Vietri M., 2009b, MNRAS, 395, 895
Caprioli D., Blasi P., Amato E., 2010a, Astropart. Phys., 33, 160
Caprioli D., Blasi P., Amato E., 2010b, Astropart. Phys., 33, 307
Chevalier R. A., Fransson C., 2006, ApJ, 651, 381
Drury L. O'C., 2011, MNRAS, 415, 1807
Drury L. O'C., Downes T. P., 2012, MNRAS, 427, 2308
Drury L. O'C., Falle S. A. E. G., 1986, MNRAS, 222, 353
Ellison D. C., Bykov A. M., 2011, ApJ, 731, 87
Ellison D. C., Eichler D., 1984, ApJ, 286, 691
Ellison D. C., Jones F. C., Eichler D., 1981, J. Geophys., 50, 110
Ellison D. C., Slane P., Patnaude D. J., Bykov A. M., 2012, ApJ, 744, 39
Gaisser T. K., Protheroe R. J., Stanev T., 1998, ApJ, 492, 219
Hillas A. M., 1984, ARA&A, 22, 425
Hillas A. M., 2005, J. Phys. G, 31, R95
Hillas A. M., 2006, J. Phys. Conf. Ser., 47, 168
Hinton J. A., Hofmann W., 2010, ARA&A, 47, 523
Johnston T. W., 1960, Phys. Rev., 120, 1103
Krymskii G. F., 1977, Sov. Phys. Dokl., 23, 327
Kulsrud R., Pearce W. P., 1969, ApJ, 156, 445
Lagage O., Cesarsky C. J., 1983a, A&A, 118, 223
Lagage O., Cesarsky C. J., 1983b, ApJ, 125, 249
Lucek S. G., Bell A. R., 2000, MNRAS, 314, 65
Malkov M. A., Diamond P. H., 2009, ApJ, 692, 1571
Malkov M. A., Diamond P. H., Völk H. J., 2000, ApJ, 533, L171
Manchester R. N., Gaensler B. M., Wheaton V. C., Staveley-Smith L., Tzioumis A. K., Bizunok N. S., Kesteven M. J., Reynolds J. E., 2002, PASA, 19, 207
Ohira Y., Mirase K., Yamazaki R., 2010, A&A, 513, A17
Ptuskin V. S., Zirakashvili V. N., 2003, A&A, 403, 1
Ptuskin V. S., Zirakashvili V. N., 2005, A&A, 429, 755
Ptuskin V. S., Zirakashvili V. N., Seo E.-S., 2010, ApJ, 718, 32
Reville B., Bell A. R., 2012, MNRAS, 419, 2433
Reville B., Bell A. R., 2013, MNRAS, preprint (arXiv:1301.3173)
Reville B., Kirk J. G., Duffy P., 2009, ApJ, 694, 951
Rogachevskii I., Kleeorin N., Brandenburg A., Eichler D., 2012, ApJ, 753, 6
Schure K. M., Bell A. R., 2011, MNRAS, 418, 782
Schure K. M., Bell A. R., Drury L. O'C., Bykov A. M., 2012, Space Sci. Rev., 173, 491
Stage M. D., Allen G. E., Houck J. C., Davis J. E., 2006, Nature Phys., 2, 614
Thomas A. G. R., Tzoufras M., Robinson A. P. L., Kingham R. J., Ridgers C. P., Sherlock M., Bell A. R., 2012, J. Comput. Phys., 231, 1051
Tzoufras M., Bell A. R., Norreys P. A., Tsung F. S., 2011, J. Comput. Phys., 230, 6475
Uchiyama Y., Aharonian F. A., Tanaka T., Takahashi T., Maeda Y., 2007, Nat, 449, 576
Vink J., 2006, in Wilson A., ed., Proc. The X-ray Universe 2005 (ESA SP-604), X-ray High Resolution and Imaging Spectroscopy of Supernova Remnants. ESA, Noordwijk, p. 319
Vink J., Laming J. M., 2003, ApJ, 584, 758
Vladimirov A., Ellison D. C., Bykov A., 2006, ApJ, 652, 1246
Völk H. J., Biermann P., 1988, ApJ, 333, L65
Völk H. J., Berezhko E. G., Ksenofontov L. T., 2005, A&A, 433, 229
Weibel E. S., 1959, Phys. Rev. Lett., 2, 83
Wentzel D. G., 1974, ARA&A, 12, 71
Zirakashvili V. N., Ptuskin V. S., 2008, ApJ, 678, 939
Zirakashvili V. N., Ptuskin V. S., Völk H. J., 2008, ApJ, 678, 255

APPENDIX A: THE VALUE OF η

The CR electric current $\boldsymbol{j}_{\rm CR}$ drives the amplification of magnetic field through the NRH instability. Throughout this paper, we express $j_{\rm CR}$ as a fraction of the CR current needed to carry the characteristic energy flux $\rho u_{\rm s}^3$: $j_{\rm CR} = \eta\rho u_{\rm s}^3/T$, where T is the characteristic CR energy in eV. In this appendix, we briefly explain why we choose $\eta \approx 0.03$ as our best estimate (see also Bell 2004).

In the absence of CR acceleration the thermal energy density downstream of a strong shock is $9\rho u_{\rm s}^2/8$ from the Rankine–Hugoniot relations. Assuming that a third of this energy is given to CRs as required for efficient CR production by SNRs, the downstream CR energy density is $3\rho u_{\rm s}^2/8$. From continuity across the shock the CR energy density immediately ahead of the shock is

also $3\rho u_s^2/8$ and the CR energy flux relative to the upstream plasma is $3\rho u_s^3/8$. However, only the highest energy CRs escape upstream. Lower energy CRs do not penetrate far upstream and they amplify magnetic field on too small a scale to engage the escaping CRs. Hence, the analysis in this paper depends on the current carried only by high-energy CRs. For a T^{-2} CR energy spectrum extending from $T_{\rm min} \approx 1\,$GeV to $T_{\rm max} \approx 1\,$PeV, the energy is spread equally across each decade in energy with a fraction $1/\ln(T_{\rm max}/T_{\rm min}) \approx 1/14$ associated with any energy T. The energy flux carried by CRs with energy T is then $\sim 3\rho u_s^3/8\ln(T_{\rm max}/T_{\rm min}) \sim 0.03\rho u_s^3$. The energy flux carried by CRs streaming at velocity v with number density $n_{\rm CR}$ and energy eT is $n_{\rm CR} veT = j_{\rm CR}T$. Consequently, we assume that $j_{\rm CR} = \eta\rho u_s^3/T$, where $\eta \sim 0.03$.

APPENDIX B: THE DERIVATION OF EQUATION (2)

Equation (2) for the electric current $j_{\rm CR}$ carried by escaping CRs assumes (i) that CRs escape upstream in a small range of momenta just above $p_{\rm max}$; (ii) that any CRs reaching a momentum $p_{\rm max}$ or higher freely stream ahead of the shock at a velocity much greater than the shock velocity u_s; and (iii) that escape is predominantly upstream. The electric current density is

$$j_{\rm CR} = e\int_{p_{\rm max}}^{\infty} \frac{4\pi}{3} f_1 c p^2\,{\rm d}p, \tag{B1}$$

where $f_1 p_r/p$ is the anisotropic part of the distribution function representing CR drift in the r direction. In a steady state on an acceleration time-scale $\partial f_0/\partial t$ can be neglected from equation (11a). The second term $\partial(f_0 u_i)/\partial r_i$ can also be neglected since the CRs are assumed to be freely streaming at energies above $cp_{\rm max}$ and advection at the fluid velocity is small. In one spatial dimension r equation (11a) then reduces to

$$-\frac{c}{3}\frac{\partial f_1}{\partial r} + \frac{\partial u}{\partial r}\frac{1}{3p^2}\frac{\partial(p^3 f_0)}{\partial p} = 0 \tag{B2}$$

for energies above $cp_{\rm max}$. Integrating in space across the shock and in momentum from $p_{\rm max}$ upwards gives

$$j_{\rm CR} = e\Delta u \frac{4\pi}{3} p^3 f_0(p_{\rm max}), \tag{B3}$$

where Δu is the change in velocity across the shock. Since $\Delta u = 3u_s/4$ for a strong shock,

$$j_{\rm CR} = e\pi u_s p^3 f_0(p_{\rm max}) \tag{B4}$$

as in equation (2).

APPENDIX C: THE DERIVATION OF EQUATIONS (12) AND (13)

Here we show how equation (12) and its vector equivalent can be derived from equations (11). For simplicity we omit terms representing advection at the fluid velocity and the effect of the magnetic field. These can easily be inserted at the end of the derivation. The difficult part is the replacement of the stress tensor f_{ij} by the vector g_i. The most transparent way of presenting the derivation is to write it out in terms of individual components in the x, y and z directions. In the following, we present the derivation of the equation for $\partial f_x/\partial t$. The derivations of the equations for $\partial f_y/\partial t$ and $\partial f_z/\partial t$ follow the same pattern. In component form, the relevant equations (11) are

$$\begin{aligned}
\frac{\partial f_0}{\partial t} &= -\frac{c}{3}\left(\frac{\partial f_x}{\partial x} + \frac{\partial f_y}{\partial y} + \frac{\partial f_z}{\partial z}\right),\\
\frac{\partial f_x}{\partial t} &= -c\frac{\partial f_0}{\partial x} - \frac{2c}{5}\left(\frac{\partial f_{xx}}{\partial x} + \frac{\partial f_{xy}}{\partial y} + \frac{\partial f_{xz}}{\partial z}\right),\\
\frac{\partial f_{xx}}{\partial t} &= \frac{c}{3}\left(-2\frac{\partial f_x}{\partial x} + \frac{\partial f_y}{\partial y} + \frac{\partial f_z}{\partial z}\right),\\
\frac{\partial f_{xy}}{\partial t} &= -\frac{c}{2}\left(\frac{\partial f_x}{\partial y} + \frac{\partial f_y}{\partial x}\right),\\
\frac{\partial f_{xz}}{\partial t} &= -\frac{c}{2}\left(\frac{\partial f_x}{\partial z} + \frac{\partial f_z}{\partial x}\right).
\end{aligned} \tag{C1}$$

Eliminating the components of the stress tensor between these equations gives

$$\begin{aligned}
\frac{\partial^2 f_x}{\partial t^2} + \frac{9c}{5}\frac{\partial}{\partial t}\frac{\partial f_0}{\partial x} &= \frac{c^2}{5}\left(\frac{\partial^2 f_x}{\partial x^2} + \frac{\partial^2 f_x}{\partial y^2} + \frac{\partial^2 f_x}{\partial z^2}\right)\\
&\quad -\frac{c^2}{5}\frac{\partial}{\partial x}\left(\frac{\partial f_x}{\partial x} + \frac{\partial f_y}{\partial y} + \frac{\partial f_z}{\partial z}\right)
\end{aligned} \tag{C2}$$

which is the x component of the vector equation

$$\frac{\partial^2 \boldsymbol{f}_1}{\partial t^2} + \frac{9c}{5}\frac{\partial(\nabla f_0)}{\partial t} = -\frac{c^2}{5}\nabla\times(\nabla\times\boldsymbol{f}_1) \tag{C3}$$

and the same derivation holds for the y and z components of the equation. This equation is second order in time differential. It can be separated into two first-order equations:

$$\begin{aligned}
\frac{\partial \boldsymbol{f}_1}{\partial t} &= -\frac{9c}{5}\nabla f_0 - \frac{c}{5}\nabla\times\boldsymbol{g}_1,\\
\frac{\partial \boldsymbol{g}_1}{\partial t} &= c\nabla\times\boldsymbol{f}_1.
\end{aligned} \tag{C4}$$

These equations become equations (12) and (13) with the addition of fluid advection, rotation of $\boldsymbol{f}_1$ by the magnetic field, and damping of the stress tensor at a rate ν_B as discussed above equation (12) in Section 4.

Note the analogy of $\boldsymbol{f}_1$ and $\boldsymbol{g}_1$ in the above equations with $\boldsymbol{E}$ and $\boldsymbol{B}$ in Maxwell's equations. In both cases, they support transverse waves.

APPENDIX D: THE APPROXIMATE CR EQUATIONS: PROPAGATING MODES

Here we demonstrate that the equations set out in Section 4 describe the essential CR propagation modes for monenergetic CRs. For simplicity we neglect the damping term ($\nu_B = 0$). Propagating CR solutions in a stationary background plasma can be found by setting $\boldsymbol{u} = 0$, $\partial/\partial r_i \to {\rm i}k_i$ and $\partial/\partial t \to -{\rm i}\omega$ in equation (13):

$$\begin{aligned}
\omega f_0 &= \frac{c}{3}k_l f_l,\\
\omega f_i &= \frac{9c}{5}k_i f_0 + \frac{c}{5}\epsilon_{ijk}k_j g_k - {\rm i}\epsilon_{ijk}\Omega_j f_k,\\
\omega g_m &= -c\epsilon_{mpq}k_{\rm p} f_q.
\end{aligned} \tag{D1}$$

The resulting dispersion relation is

$$\begin{aligned}
&\left(\omega^2 - \frac{3c^2k^2}{5}\right)\left\{\left(\omega^2 - \frac{c^2k^2}{5}\right)^2 - \omega^2\Omega^2\right\}\\
&\qquad -\frac{2k^2c^2}{5}\omega^2\Omega^2\sin^2\theta = 0\,,
\end{aligned} \tag{D2}$$

where θ is the angle between $\boldsymbol{k}$ and $\boldsymbol{B}$. There are two independent modes in the absence of magnetic field ($\Omega = 0$). The mode propagating at $\sqrt{3/5}c$ represents the motion of freely propagating CRs with $\boldsymbol{f}_1$ parallel to $\boldsymbol{k}$. The mode propagating at $\sqrt{1/5}c$ is the transverse mode representing the motions of CRs with $\boldsymbol{f}_1$ perpendicular to $\boldsymbol{k}$. The transverse mode propagates more slowly because CR velocities are aligned preferentially away from the direction of propagation.

In the presence of a magnetic field, a longitudinal mode still propagates parallel to $\boldsymbol{B}$ ($\theta = 0$) at $\sqrt{3/5}c$ representing free propagation along field lines unaffected by the field. The transverse mode is relatively unaffected by the magnetic field at wavelengths shorter than a Larmor radius $kc \gg \Omega$. At wavelengths longer than the Larmor radius, the transverse mode propagates more slowly as the transverse CR current rotates rapidly in the magnetic field.

When mode propagation is directed across the magnetic field ($\sin\theta = 1$), the wave frequency is given by

$$\omega^2 = \Omega^2 \left\{ \frac{1}{2} + \frac{2k^2 r_{\rm g}^2}{5} \pm \sqrt{\frac{1}{4} + \frac{k^4 r_{\rm g}^4}{25} + \frac{2k^2 r_{\rm g}^2}{5}} \right\}, \tag{D3}$$

where $r_{\rm g}$ is the CR Larmor radius. In the limit of wavelengths smaller than the Larmor radius, the frequency converges to those derived for the longitudinal and transverse waves in zero magnetic field as expected. At long wavelengths ($kr_{\rm g} \ll 1$), the frequency converges to the Larmor frequency, representing CR rotation in the magnetic field, without significant propagation.

This analysis of the dispersion relation indicates that equations (13) for f_0, $\boldsymbol{f}_1$ and $\boldsymbol{g}_1$ provide an adequate representation of CR propagation.

APPENDIX E: THE APPROXIMATE CR EQUATIONS: THE NRH INSTABILITY

We now investigate whether the approximate treatment of CR kinetics in Section 4 is adequate to model the NRH instability. We derive the dispersion relation for the NRH instability in a simple case with the following assumptions. The CRs are monoenergetic with momentum p. The zeroth-order CR current $\boldsymbol{j}_0$, the wavenumber $\boldsymbol{k}$ and the zeroth-order magnetic field $\boldsymbol{B}_0$ are all parallel. The background plasma is at rest to zeroth order, $\boldsymbol{u}_0 = 0$. The first-order perturbations to the magnetic field $\boldsymbol{B}_1$, CR current $\boldsymbol{j}_1$ and plasma velocity $\boldsymbol{u}_1$ are all perpendicular to the zeroth-order magnetic field and the wavevector $\boldsymbol{k}$. Since the modes are transverse, the plasma density is unperturbed to first order: $\rho_1 = 0$. The coupled linearized forms of equations (7), (13) and the Maxwell equation for $\partial\boldsymbol{B}/\partial t$ are then

$$\begin{aligned}
\rho\frac{\partial \boldsymbol{u}_1}{\partial t} &= -\boldsymbol{j}_0 \times \boldsymbol{B}_1 - \boldsymbol{j}_1 \times \boldsymbol{B}_0 + \frac{1}{\mu_0}(\boldsymbol{B}_0 \cdot \nabla)\boldsymbol{B}_1 , \\
\frac{\partial \boldsymbol{B}_1}{\partial t} &= (\boldsymbol{B}_0 \cdot \nabla)\boldsymbol{u}_1 , \\
\frac{\partial \boldsymbol{j}_1}{\partial t} &= -\frac{c}{5}\nabla \times \boldsymbol{G}_1 - \frac{ec}{p}\boldsymbol{B}_0 \times \boldsymbol{j}_1 - \frac{ec}{p}\boldsymbol{B}_1 \times \boldsymbol{j}_0 , \\
\frac{\partial \boldsymbol{G}_1}{\partial t} &= c\nabla \times \boldsymbol{j}_1 - \nu_B \boldsymbol{G}_1 ,
\end{aligned} \tag{E1}$$

where $\boldsymbol{G}_1 = (4\pi/3)ec \int p^2 \boldsymbol{g}_1 \mathrm{d}p$. For circular polarization any first-order perturbation $\boldsymbol{\xi}_1$ ($\boldsymbol{B}_1$, $\boldsymbol{j}_1$, $\boldsymbol{G}_1$ or $\boldsymbol{u}_1$) satisfies

$$\frac{\partial \boldsymbol{\xi}_1}{\partial t} = -\omega \boldsymbol{n} \times \boldsymbol{\xi}_1 ; \qquad (\boldsymbol{n} \cdot \nabla)\boldsymbol{\xi}_1 = k\boldsymbol{n} \times \boldsymbol{\xi}_1 , \tag{E2}$$

where $\boldsymbol{n}$ is a unit vector in the direction of $\boldsymbol{B}_0$, giving

$$\begin{aligned}
-\rho\omega \boldsymbol{u}_1 &= -j_0 \boldsymbol{B}_1 + B_0 \boldsymbol{j}_1 + \frac{kB_0}{\mu_0}\boldsymbol{B}_1 , \\
-\omega \boldsymbol{B}_1 &= kB_0 \boldsymbol{u}_1 , \\
-\omega \boldsymbol{j}_1 &= -\frac{ck}{5}\boldsymbol{n} \times \boldsymbol{G}_1 - \frac{ecB_0}{p}\boldsymbol{j}_1 + \frac{ecj_0}{p}\boldsymbol{B}_1 , \\
-\omega \boldsymbol{G}_1 &= ck\boldsymbol{n} \times \boldsymbol{j}_1 + \nu_B \boldsymbol{n} \times \boldsymbol{G}_1 .
\end{aligned} \tag{E3}$$

As discussed in Section 4, we set the scattering frequency ν_B equal to the CR Larmor frequency. For SNR conditions, the NRH growth rate ($\sim\Gamma$) is much less than the CR Larmor frequency, in which case the dispersion relation simplifies to

$$\omega^2 \approx k^2 v_{\rm A}^2 - \sigma_\pm \Gamma^2 \left(1 \pm \frac{5\mathrm{i}}{k^2 r_{\rm g}^2} \right)^{-1} , \tag{E4}$$

where $v_{\rm A} = \sqrt{B_0^2/\rho\mu_0}$ is the Alfvén speed, $r_{\rm g}$ is the CR Larmor radius in the magnetic field B_0 and $\Gamma = \sqrt{kB_0 j_0/\rho}$ is the NRH growth rate where it dominates in the range $r_{\rm g}^{-1} \ll k \ll \Gamma/v_{\rm A}$. $\sigma_\pm = \pm 1$ according to the sense of the circular polarization as determined by the sign of k.

For wavelengths much shorter than the Larmor radius ($kr_{\rm g} \gg 1$)

$$\omega^2 = k^2 v_{\rm A}^2 - \sigma_\pm \Gamma^2 \tag{E5}$$

which represents a purely growing instability for wavenumbers less than $\Gamma/v_{\rm A}$ in the appropriate polarization $\sigma_\pm = 1$. Tension in the magnetic field correctly damps waves with wavenumbers greater than $\Gamma/v_{\rm A}$ (Bell 2004). The truncated tensor analysis is correct on scales smaller than the Larmor radius because CR trajectories are then relatively unaffected by perturbations in the magnetic field. This is the important regime in which the rapidly growing NRH instability amplifies the magnetic field.

At wavelengths longer than the Larmor radius ($kr_{\rm g} \ll 1$), the approximate tensor expansion gives

$$\omega^2 = k^2 v_{\rm A}^2 \pm \mathrm{i}\frac{k^2 r_{\rm g}^2}{5}\Gamma^2 . \tag{E6}$$

In comparison the correct dispersion relation in this limit is $\omega^2 = k^2 v_{\rm A}^2 - k^2 r_{\rm g}^2 \Gamma^2/5$ for the resonant instability and $\omega^2 = k^2 v_{\rm A}^2 + k^2 r_{\rm g}^2 \Gamma^2/5$ for the non-resonant instability which in fact is stable for monoenergetic CRs in this limit. The Alfvén term $k^2 v_{\rm A}^2$ is negligible at long wavelengths so the tensor expansion gives a growing mode with

$$\omega = \frac{\mathrm{i} \pm 1}{\sqrt{10}}(kr_{\rm g})\Gamma \tag{E7}$$

in both resonant and non-resonant polarizations.

Fig. E1 compares the approximate tensor dispersion relation (top row) with the correct dispersion relations of Bell (2004) (bottom row) for both the resonant instability ($\sigma_\pm = -1$) that dominates for $kr_{\rm g} < 1$ and the rapidly growing non-resonant NRH instability ($\sigma_\pm = -1$) that dominates for $kr_{\rm g} > 1$. Crucially, the tensor expansion accurately calculates the NRH growth rate in the range $r_{\rm g}^{-1} < k < \Gamma/v_{\rm A}$. Outside this range, the growth rate is too small for the instability to be effective. The tensor expansion reproduces the growth of the resonant instability for $kr_{\rm g} < 1$ although it incorrectly produces weak growth of the non-resonant instability in this regime. The crucial point for the simulation is that the tensor expansion gives an accurate account of instability where the growth rate is large.

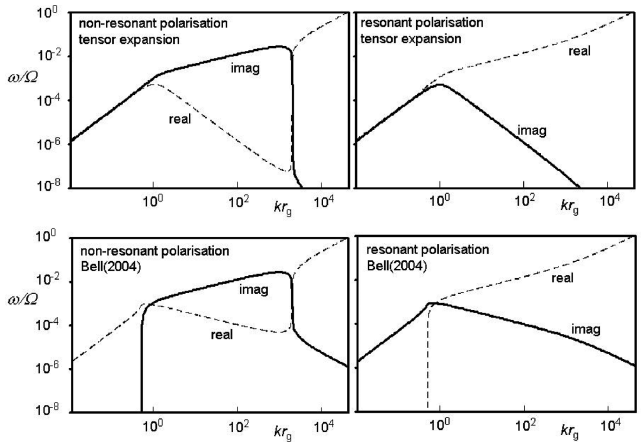

Figure E1. Dispersion relation for the resonant and non-resonant circular polarizations as derived from the tensor expansion (top row) compared with the dispersion relation derived by Bell (2004) for monoenergetic CRs (bottom row). The growth rates in units of the CR Larmor frequency are given by the full lines and the real frequencies by the dashed lines. Parameters relevant to the historical SNR are assumed.

APPENDIX F: COMPUTATIONAL CONSTRAINTS

The simulation makes heavy demands on computational resources because it models spatial scales encompassing the wavelength of the fastest growing mode, the CR Larmor radius and the free propagation of CRs ahead of the shock. It is three dimensional in configuration space and models the CR distribution in momentum. The spatial cell size Δx must be small enough to allow the NRH instability to grow from its initially small scale ($\Delta x < \pi/k_{\rm max}$) and the time-step Δt must be short enough to resolve CRs crossing one computational cell ($\Delta t < \Delta x/c$). The simulation must be run for a time τ at least 10 times the growth time of the fastest growing mode $\tau = 10\gamma_{\rm max}^{-1}$, and the length of the computational grid $L_{||}$ in the direction parallel to the shock normal must be large enough to allow the CRs to escape upstream: $L_{||} = 10c\gamma_{\rm max}^{-1}$. Provided the boundary conditions are periodic in the directions perpendicular to the shock normal, they can be much smaller than $L_{||}$ but they must be able to accommodate a CR Larmor radius: $L_\perp = r_{\rm g}$. The number of computational operations is proportional to $N_{\rm comp} = \tau L_{||} L_\perp^2/(\Delta t \Delta x^3)$, which from definitions and equations presented above is of order

$$N_{\rm comp} \sim \frac{\eta^2 M_{\rm A}^6}{4}\,. \tag{F1}$$

As discussed above, the NRH instability grows strongly in a wavenumber range between $r_{\rm g}^{-1}$ and $k_{\rm max}$. Saturation due to magnetic tension occurs on scalelengths comparable to the CR Larmor radius $r_{\rm g,\,sat}$ when $B_{\rm sat}/r_{\rm g,\,sat} = \mu_0 j_{\rm CR}$ as discussed in Section 10. The ratio of the saturated field $B_{\rm sat}$ to the initial field B_0 is $B_{\rm sat}/B_0 = (2r_{\rm g}k_{\rm max})^{1/2}$, where $k_{\rm max}$ and $r_{\rm g}$ are defined in the initial field B_0. The equation for $k_{\rm max}$ can be found in Section 2, giving

$$B_{\rm sat}/B_0 \sim M_{\rm A}\sqrt{\frac{\eta u_{\rm s}}{c}}\,, \tag{F2}$$

where the acceleration efficiency η is also defined in Section 2. The Alfvén Mach number $M_{\rm A}$ must be large to allow significant amplification of the magnetic field ($B_{\rm sat} \gg B_0$). From equation (F1) large $M_{\rm A}$ imposes a heavy demand on computational resources, but from equation (F2) the cost can be minimized by making the shock velocity $u_{\rm s}$ a large fraction of the speed of light. We initiate the simulation with an unrealistically large magnetic field of 47 μG to reduce the Alfvén Mach number from its typical value of ∼1000 for shocks in young SNRs.

This paper has been typeset from a TEX/LATEX file prepared by the author.